MODELING OF IEEE 34 NODE RADIAL DISTRIBUTION FEEDER WITH DISTRIBUTED GENERATION IN REAL TIME ENVIRONMENT USING OPAL-RT™ SIMULATOR

Thesis submitted in the partial fulfilment of the requirements for the degree of

MASTER OF ELECTRICAL ENGINEERING

SUBMITTED BY

DEEPESH DAS

Examination Roll No.: M4ELE19006

Registration No.: 140666 of 2017-18

Under the Guidance of

Mr. AYAN KUMAR TUDU

Assistant Professor
Department of Electrical Engineering
Faculty of Engineering and Technology
Jadavpur University
Kolkata, West Bengal - 700032

2019

DEDICATED TO MY PARENTS

AND

MY LATE GRANDPARENTS

Faculty of Engineering & Technology

JADAVPUR UNIVERSITY

KOLKATA- 700032

Certificate of Recommendation

This is to certify that Shri. Deepesh Das has completed his project work entitled **"Modeling Of IEEE 34 Node Radial Distribution Feeder With Distributed Generation In Real Time Environment Using Opal-RT™ Simulator"** under my direct supervision and guidance. This thesis is submitted in partial fulfilment of the requirements for the award of degree of Master of Electrical Engineering during the academic year 2017-2019.

_____

Mr. Ayan Kumar Tudu
Assistant Professor
Dept. of Electrical Engineering
Faculty of Engineering and Technology
Jadavpur University

Forwarded by:

_____

Dr. Kesab Bhattacharyya
Head
Dept. of Electrical Engineering
Faculty of Engineering and Technology
Jadavpur University

_____

Dr. Chiranjib Bhattacharjee
Dean
Faculty of Engineering and Technology
Jadavpur University

Faculty of Engineering & Technology

JADAVPUR UNIVERSITY

KOLKATA- 700032

*Certificate of Approval **

The foregoing thesis is hereby approved as a credible study of **Master of Electrical Engineering** and presented in a manner satisfactory to warrant its acceptance as a prerequisite to the degree for which it has been submitted. It is understood that by this approval the undersigned do not necessarily endorse or approve any statement made, opinion expressed or conclusion therein but approve this thesis only for the purpose for which it is submitted.

Final Examination for
Evaluation of the Thesis

_____

_____

Signature of the Examiners

*Only in case the thesis is approved

Declaration of Originality and Compliance of Academic Ethics

I hereby declare that this thesis contain literature survey and original research work by the undersigned candidate, as part of **Master of Electrical Engineering** studies.

All information in this document have been obtained and presented in accordance with academic rules and ethical conduct.

I also declare that, as required by these rules and conduct, I have fully cited and referenced all material and results that are not original to this work.

Name	:	**DEEPESH DAS**
Exam Roll Number	:	**M4ELE19006**
Thesis Title	:	**MODELING OF IEEE 34 NODE RADIAL DISTRIBUTION FEEDER WITH DISTRIBUTED GENERATION IN REAL TIME ENVIRONMENT USING OPAL-RT^{TM} SIMULATOR**

Signature with date :

ACKNOWLEDGEMENT

It is a pleasure to express my gratitude to all those people who have accompanied and helped me in my project work.

First and foremost, I take this opportunity to express my gratitude to my guide, Mr. Ayan Kumar Tudu, Assistant Professor, Department of Electrical Engineering, Jadavpur University, Kolkata, for his invaluable guidance, suggestions and encouragement throughout the project, which helped me a lot to improve this project work. It has been a wonderful experience to be under his guidance. His appreciation and direction has been a source of moral encouragement and confidence.

I am also indebted to Dr. Kesab Bhattacharyya, Head, Department of Electrical Engineering, Jadavpur University, for his kind help during this thesis work. I am also thankful to Dr. Chiranjib Bhattacharjee, Dean of Faculty of Engineering and Technology for his kind help and cooperation during this thesis work.

I am also indebted to my parents and my loved ones who encouraged me to give my best effort during this thesis work.

Last, but not the least, I would like to thank my batchmates who have directly or indirectly helped me in this work.

Deepesh Das
Dept. of Electrical Engineering
Jadavpur University
Kolkata-700032

CONTENTS

ABSTRACT

The need for distributed generation (DG) is becoming more and more evident in recent times as a primary requirement for smart electricity distribution planning and also to cater ever increasing load demand. This thesis presents a study on the modelling of existing IEEE 34 Node Radial Distribution Feeder with the addition of DG's to the feeder nodes. The system is studied in its nominal state at first to achieve the expected operation standards. Switching of DG's are made within that time span to visualize the changes in the states of the system.

The system is isolated from the main grid to study how the system performs with the help of DG's. A fault study is also performed on the system to observe how the system behaves as per the incipient fault and how the DG's can provide support in stabilising the fault. The existing IEEE 34 Node Radial Distribution Feeder was not designed with distribution generation (DG) in mind. As DG penetration is being considered by many distribution utilities, there is a rising need to address the compatibility issues that are occurring in the power system. The entire analysis has been simulated in SIMULINK/MATLAB™ environment and validated through OPAL-RT™ real time simulator.

LIST OF FIGURES

ABBREVIATIONS

DG	Distributed Generation
MW	Mega-watt
kW	Kilo-watt
kV	Kilo-volt
kVA	Kilo-Volt-Ampere
kVAr	Kilo-Volt-Ampere reactive
Km	Kilometre
IEEE	Institute of Electrical and Electronics Engineers
OLTC	On-Load Tap Changing Transformer
CB	Circuit Breaker
CIGRÉ	International Council on Large Electric Systems
CO_2	Carbon Di-oxide
FF	Form Factor
MPPT	Maximum Power Point Tracking
DC	Direct Current
AC	Alternating Current
PV	Photovoltaic
CA	Current Amplifier
PWM	Pulse Width Modulation
ACMC	Averaged Current Mode Control
RTOS	Real Time Operating System
µs	Micro-second

CHAPTER 1

INTRODUCTION

- Overview
- Literature Survey
- Objective
- Organisation of the Thesis

1.1 OVERVIEW

Distributed generation (DG) also known as distributed energy, on-site generation or district/decentralized energy is electrical generation performed by a variety of small, grid-connected or distribution system connected devices referred to as distributed energy resources.

Conventional power stations, such as coal-fired, gas, and nuclear-powered plants, as well as hydroelectric dams and large-scale solar power stations, are centralized and often require electric energy to be transmitted over long distances. By contrast, DG systems are decentralized, modular, and are made of more flexible technologies, that are located close to the load they serve, albeit having capacities of only 10 megawatts (MW) or less. These systems can comprise multiple generation and storage components; in this instance they are referred to as hybrid power systems.

DG systems typically use renewable energy sources and increasingly play an important role for the electric power distribution system. By means of an interface, DG systems can be managed and coordinated within a microgrid or a smart grid. Distributed generation enables collection of energy from many sources and may lower environmental impacts and improve security of supply. It is also the need of the time that every aspect of these kind of systems be monitored and controlled in real time.

In this work, the focus is kept on the study of the behaviour of the IEEE 34 radial distribution feeder once it is put into an islanding mode. In this mode, it is fed from DG sources and hence the behaviour of the system is studied.

1.2 LITERATURE SURVEY

With the increasing surge in load demand in modern times there is an insatiable need for electrical energy. With that comes the advent of tools in making effort to provide acceptable uninterrupted power supply. In this work, focus was made on a heavily loaded bus system viz. the IEEE 34 node radial distribution system where study was performed regarding power supply continuity in islanded mode. The general data for design of this system was found in IEEE Power Engineering Society ‘s data-sheet [1] available as an open source resource. The IEEE 34 node system was studied in detail by **Ndaga Mwakabuta** et al. [2] regarding the study of the system with asymmetrical loading and registering of data regarding comparison of voltage profiles and system losses to determine sizing, location and control parameters. This data served as superior aid in designing the system. When distributed generation was introduced in this system, it brought in new challenges regarding control of reactive power and voltage regulation to loads and distribution systems. The increase in the dynamicity of the system was studied in detail by **James O. Owuor** et al. [3] where the steady state results were obtained using DG.

The focus was on the islanding phenomenon wherein a great deal of research work was made by **Sidharth Parmar Ashok** [4] where study was a comparison between with and without DG and their effects on islanding mode. As we moved our focus on islanding mode with DG, to study the complexity a real-time simulator like OPAL-RT^{TM} was required. **Pawan Singh** [5] in his work established the structure for system design using Simulink^{TM} and simulating it in OPAL-RT^{TM} for research purpose.

Now, when in islanded mode the system was bound to behave like a microgrid. From the works of **Dr. Anitha Subburaj** et al. [6] important design references were drawn in which they discussed about microgrid

and energy storage technologies. **H. Hooshyar** et al. [7] provided an extremely elaborate design description on how to design the IEEE 34 node radial feeder and how to segregate into parts to simulate in OPAL-RT^{TM} hardware-in-the-loop.

As the modelling steps were decided a knowledge base was needed as literature reference for optimisation of data as per needs. Transmission line data conversion and modifications were made as per the literature [8] references available.

Solar energy was the choice of resource for DG and hence a congruent PV system was needed to be designed. Keeping maximum generation of power, the need for MPPT was realised. In this regard, **Sonali Surawdhaniwar** et al. [9] proposition for maximum energy generation with aid of MPPT was deemed highly necessary. The need for MPPT was further realised with work of **Yinghua Dong** et al. [10] wherein they simulated the output of efficiently using MPPT techniques in their works.

Lloyd Dixon [11] explained in the application notes a robust technique for average current mode control in boosting the voltage level which eliminates peak-to-average current errors. Furthermore, **Wei Xi** [12] in his report further emphasizes on the control element of dc-dc voltage boost converter to bring it up to the utility level.

Jenica Ilena Corcau et al. [13] presented an averaged inverter model which is used as reference for the inverter model within the PV system in this work. As a support, research work from **Mustapha Raoufi** et al [14] was referred which aimed towards harmonic reduction in simulation for both transient and steady state.

Liang Che et al [15] presented work on coordination of AC and DC microgrids wherein power levels were measured. This proved as useful reference in comparison of power flows in different situations. Data verification reference was available in the research work of **Jatin Jangra** et al. [16] research work where the IEEE 34 node radial system was simulated in MATLAB/Simulink™ environment to compare data with the empirical data available and as a tool for data verification for this work.

The solar energy data is obtained from the report [17] presented by project director **Aasha Kapur Mehta** for Ministry of New and Renewable Energy – Government of India, which provides valuable insight while developing the motives of the work performed here.

1.3 OBJECTIVE

This thesis introduces the modelling of the IEEE 34-node radial distribution feeder system structure and study the impacts of distribution resources when integrating with distribution systems. Many different distribution structures exist like networked or radial systems or based on grounding configurations. Radial distribution systems consist of a main substation with multiple feeders. They key feature about this system is it has only one source.

The IEEE 34 bus radial distribution network will be built with the existing data based on symmetrical components while keeping most of the system parameters unchanged. This is done with the addition of DG's to specific feeders which have already been studied.

Also, the goal is to study the IEEE 34 bus radial distribution feeder when tied to the main grid and in islanded mode when the power supply is provided from the DG's attached to it. The whole setup is simulated

using software tools in MATLAB™ and in real-time using the real time simulator OPAL-RT™. The results are then compared and studied.

1.4 ORGANISATION OF THE THESIS

The thesis is compiled in six chapters as per the details mentioned below:

Chapter 1 highlights on the brief introduction of the thesis presented and a list of the work that was performed in this endeavour. It also provides as an outline to the direction of the work and contains noteworthy works that provided foundation to this work.

Chapter 2 explains in detail the modelling of the IEEE 34 node radial distribution system in the MALTLAB™ Simulink™ environment. It explains in detail the choices and their reasons while designing different components of the system and what is their role in the results obtained.

The present work contains distributed generation units which play crucial roles in this work. **Chapter 3** explains in detail the procedure for designing those units and how they are implemented.

Chapter 4 explains in detail how the system was designed and simulated in OPAL-RT™ environment, coming with its own considerations.

Chapter 5 presents the results for various operating conditions.

Chapter 6 concludes the work and presents further scopes for future development works.

CHAPTER 2

MODELING THE IEEE 34-NODE DISTRIBUTION FEEDER

- Introduction
- The IEEE 34-node test feeder
- Modelling the IEEE 34-node test feeder
  - Load Model
  - Distribution Feeder line model
  - Voltage Regulator
  - Transformer, Breaker & Capacitor Bank

2.1 INTRODUCTION

A variety of computer simulation softwares are available for analysis of distribution feeders. The data from paper [1], which was used to verify the accuracy of the computer simulations, was published to make the data for radial distribution feeder available to scholars and program developers. While designing it was thoroughly noted that the concerned was an unbalanced test feeder. Several softwares are available for the analysis of unbalanced three phase radial distribution feeder. The complete data and solutions [1] for all the test feeders can be downloaded from the internet. While the literature [2,3] on the distribution system is abundant, the use of real-time simulation for these kind of setups need more contribution. The primary objective of this work includes selection, validation, and modelling of a distribution feeder along with photovoltaics in Simulink™ and RT-LAB™ for formation of a microgrid, followed by validating the model in a hardware real-time simulator OPAL-RT™.

2.2 THE IEEE 34-NODE TEST FEEDER

The reason for choosing the IEEE 34-node test feeder model [1] was that it represents an actual distribution feeder in Arizona, USA and exhibits the following interesting characteristics, which are listed as follows:

- Each section of the distribution system is modelled by actual phase impedance values.
- The system includes single- and two-phase laterals.
- Loads on each phase of each section are specified in real and reactive power.
- Distributed load models represent load on feeders with closely spaced load taps.

- System includes voltage regulators and capacitive reactive power compensation.
- The system has very long distribution lines and is lightly loaded.
- There is also an in-line transformer for reducing voltage to 4.16 kV for a short section of the feeder.

2.3 MODELLING THE IEEE 34-NODE TEST FEEDER IN SIMULINK™/ SIMPOWERSYSTEM™

TOOLS AND TECHNIQUE

Simulink™, developed by Mathworks™, is a graphical programming environment for modelling, simulating and analysing multidomain dynamical systems. Its primary interface is a graphical block diagramming tool and a customizable set of block libraries.

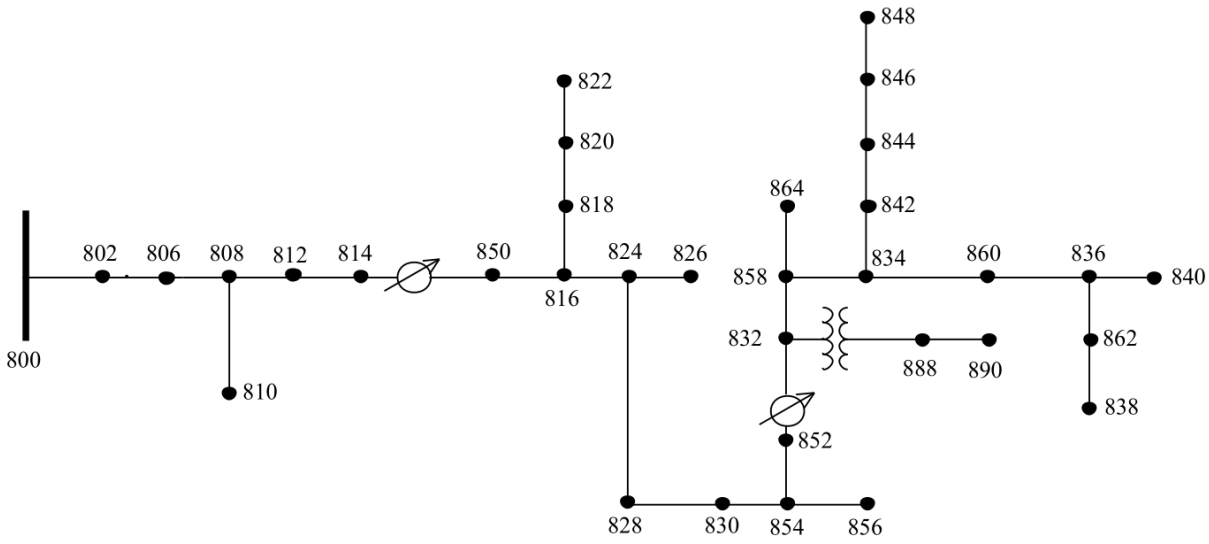

Figure 2.1: The IEEE-34 node test feeder

Simulink™ offers tight integration with the rest of the MATLAB™ environment and can either drive MATLAB™ or be scripted from it. Simulink™ is widely used in automatic control and digital signal processing for multidomain simulation and Model-Based Design.

The model components used in the model were obtained from Simulink™. Demo models were used as guides for building the model. [16] The development of the model is further described in the following sections.

2.3.1 LOAD MODEL

The IEEE 34-Node distribution feeder [1-2] consists of only static loads. Here static loads are referred to loads that do not contain any motor. Here the loads are configured as three-phase, two-phase or single-phase nature with constant PQ, I or Z load connected in delta or wye configuration. The three-phase balanced load can be modelled by using three phase series RLC load which is available under the SimPowerSystem™ library. The load real power P (W) and reactive power Q (VAr) can be specified in the model.

The 34-node distribution model requires unbalanced load models, which is modelled using series RLC load block given in Simulink™. The delta connected load rating for Phase-A, Phase-B and Phase-C refer to the ratings of the loads connected between phases A-B, B-C and C-A respectively. If not specified, the neutral is grounded by default. Figure 2.2 shows the parameters in the Simulink™ block for load configuration according to the IEEE 34-Node test data. The parameters shown are for the load at node-816 and the load is 5 kW and 2 kVAr at phase-B. This delta load is connected between phase B-C. If a single-phase load is wye configuration then it is connected between line to ground. Such an example is found at node-826 for the load of 40 kW and 20 kVAr connected between phase-B and the ground.

Also, we have unbalanced two phase loads in the model and the connection is in the fashion single phase loads are connected. Such an

example is found at node-802, for wye connected load, for the load of 30 kW and 15 kVAr at phase-B and for the load of 25 kW and 14 kVAr at phase-C, respectively connected to the ground.

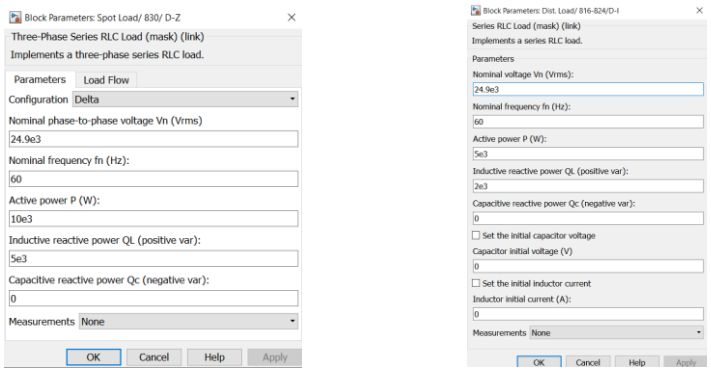

Figure 2.2: Simulink™ load model parameters

2.3.2 DISTRIBUTION FEEDER LINE MODEL

The line modelling was made using RLC elements available in Simulink™ library. As in the real world, the line provides a natural propagation delay it was intended to be introduced in the model. The IEEE 34-Node distribution system has unbalanced three-phase load and the line parameters are given in impedance and admittance matrix data. Hence, a PI-line model [5] was developed in Simulink™ with R-L in parallel with C/2 at each end using the RLC model branch model in Simulink™ as shown in Figure 2.4. This matrix element represents G+jB, where G was negligible. The line capacitance C is calculated as $C = \frac{B}{2\pi f}$. Values of R, L and B line parameters were obtained from the feeder test data.

$$z = R + j\omega L = R + jX$$

$$y = \frac{1}{Rsh} + j\omega C = G + jB$$

where, R is the series resistance (Ω/m), X is the series /m), X is the series /m), X is the series reactance (Ω/m), G is the shunt conductance (S/m), and B is the shunt susceptance (S/m).

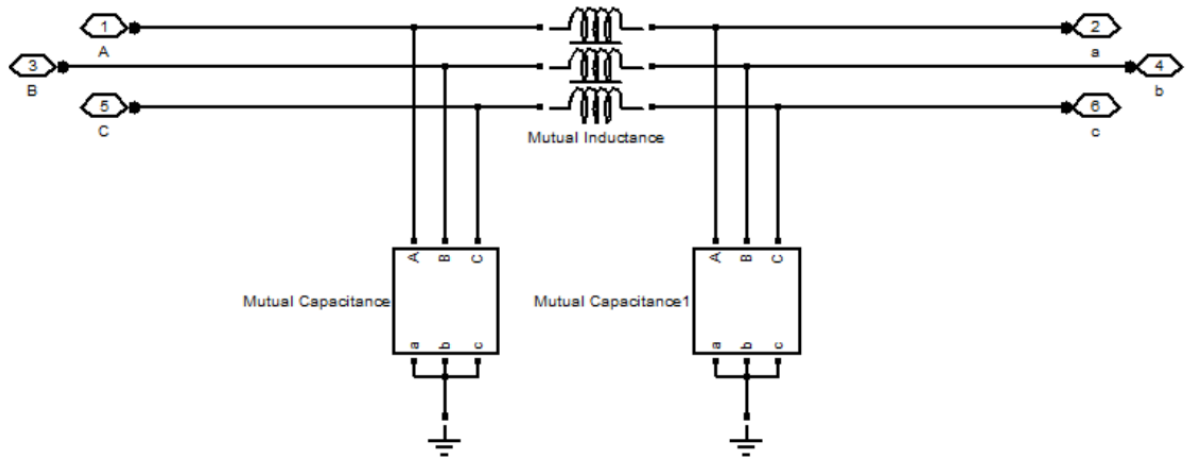

Figure 2.3: Three-phase pi line model

The IEEE 34-Node distribution feeder test data provide data for impedance and admittance matrix. The data required was modified to feed into the model parameters as shown in Appendix A.3. The line parameter values of R, L and C varies as per the configuration of the line as shown in Appendix A.1. Such an example is cited in Figure 2.2.

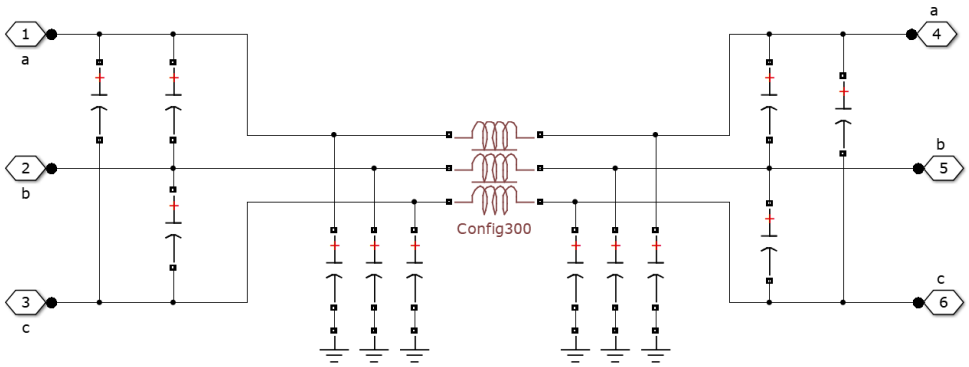

Figure 2.4: Distribution feeder line section model

The values of line lengths were given in feet while the parameters for the line components were given in units per mile. But, MATLAB™

parameters take values in only S.I. units. So, the values were needed to be changed into kilometres(km).

It is known, 1 mile = 1.609344 km ≈ 1.6 km

1mile = 5280 feet

The conversion is made whenever the line section values are used. E.g. for the line section between bus no. 824 and 826, such a modification is done as shown in Figures 2.5 and 2.6. Line section length is 3030 feet.

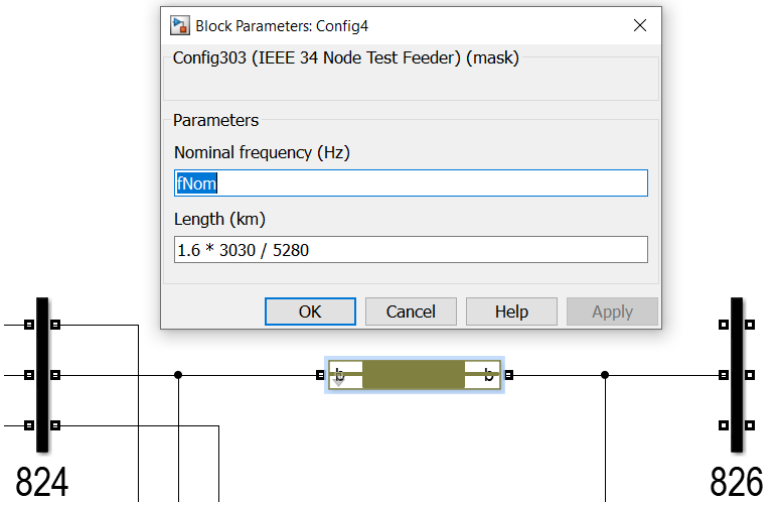

Figure 2.5: External view of line section

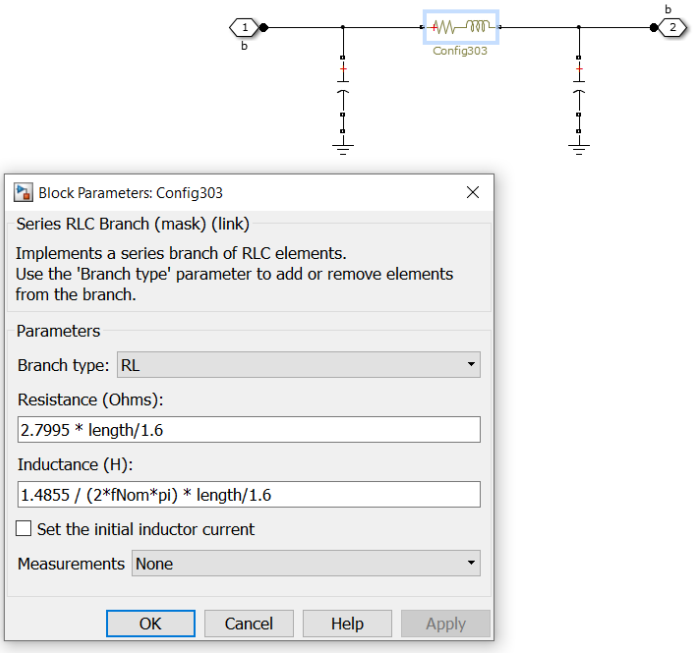

Figure 2.6: Internal view of line section

The above-mentioned was for a single-phase line. But most of the feeder consists of three phase transmission lines whose configuration is as shown in Figure 2.7. The value for the feeder section is obtained from the IEEE data for the test feeder. The values for the R, L and C is provided in the matrix format. The mutual inductance and the resistance associated with it is represented in the series format and the values are entered into the parameters as inductance matrix and resistance matrix. But the capacitance is represented as a shunt parameter. For the three-phase line section the values of the capacitances are obtained. The capacitance naturally occurs between the phases to the ground and between different phases. For Figure 2.6, the data obtained were in the form of:

B_{AA} = 5.3350 µS, B_{AB} = -1.5313 µS and B_{AC} = -0.9943 µS

So, $B_{A0} = B_{AA} + B_{AB} + B_{AC}$ = 2.8094 µS

So, Capacitance between phase A and ground = $B_{A0} / (2 * \pi * f)$ = 8.9426 nC details of which can be found in Appendix A.3.

Now, the parameter of capacitance and inductances are free from the system frequency (f) and hence the model can be put into use for any system frequency.

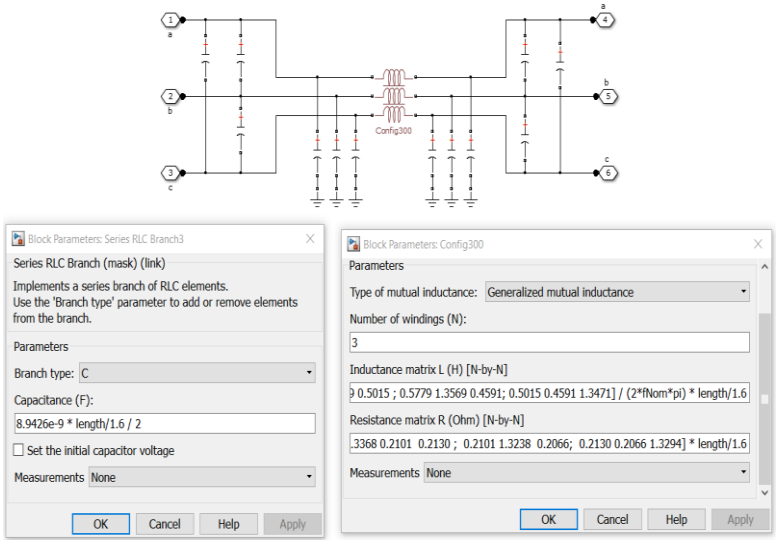

Figure 2.7: Parameters for transmission line section

2.3.3 VOLTAGE REGULATOR

A step-voltage regulator consists of an autotransformer and a load tap changing mechanism. A standard step regulator contains a reversing switch enabling ±10% regulator usually in 32 steps, which amount to 5/8% change in voltage.

In this work, the study was focused on the construction of the IEEE 34-Node test feeder and various simplifications were made. The OLTC so considered as the voltage regulator medium was modelled by Three-Phase Transformers (Two Windings) which is available in Simulink™ library under SimPowerSystems™, as shown in Figure 2.8.

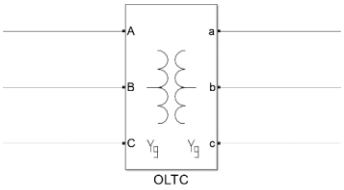

Figure 2.8: On-Load Tap Changing Transformer block

2.3.4 TRANSFORMER, BREAKER, AND CAPACITOR BANK

The system model included transformer, circuit breakers and capacitor banks for study. The three-phase transformer was represented by Three-Phase Transformers (Two Windings) available in Simulink™ under SimPowerSystems™. The values of rms line-line voltage, system frequency, pu resistance and pu reactance and type of transformer winding connections were provided as parameters as shown in Figure 2.9. These values were obtained from the IEEE 34-Node test feeder data.

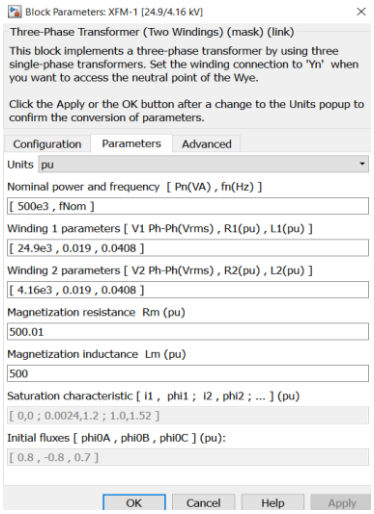

Figure 2.9: Transformer parameters

Capacitor banks were modelled by the Three-Phase Series RLC Load block found in Simulink™ under SimPowerSystems™. The capacitor bank, capacitive reactive power (VAr) value was obtained from the IEEE 34-Node test feeder data. In the block the active power and the inductive reactive power values were set to zero as shown in Figure 2.10, where V_n is the rms line-line voltage, f_n is the system frequency and Q_c is the capacitive reactive power. All capacitor banks in this system have been connected in star grounded connection.

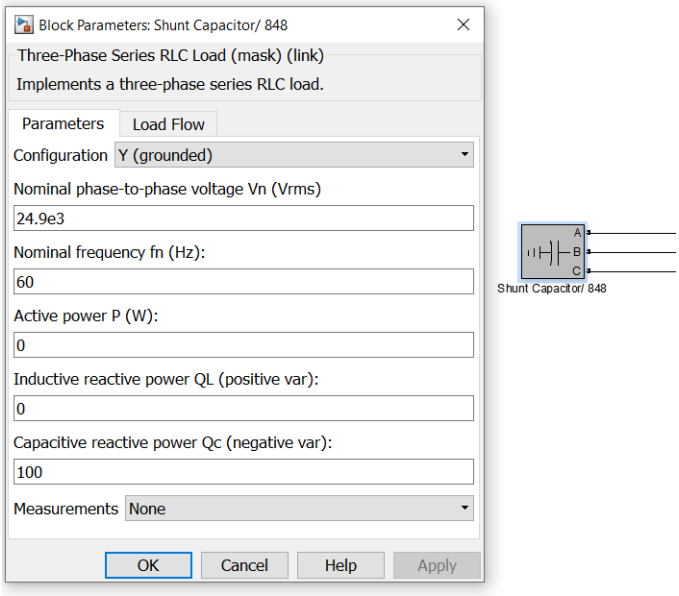

Figure 2.10: Capacitor Bank parameters

Circuit breakers were implemented to connect or disconnect the photovoltaic microgrids to the IEEE 34-Node test system. The CBs were represented by Three-Phase Breaker block available in Simulink™ under SimPowerSystems™. The switching times were provided as parameters depending on the choice and needs of the tests performed. The CBs are implemented as shown in Figure 2.11.

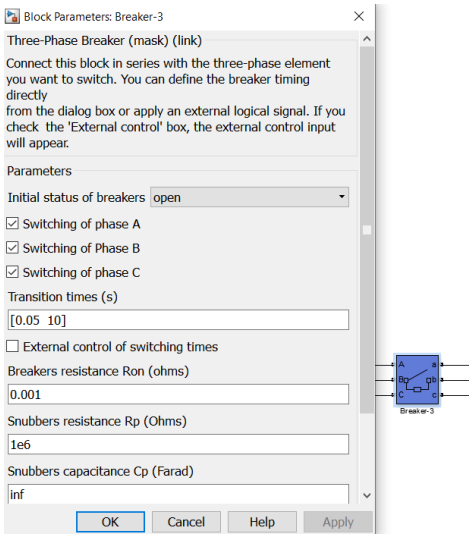

Figure 2.11: Circuit Breaker parameters

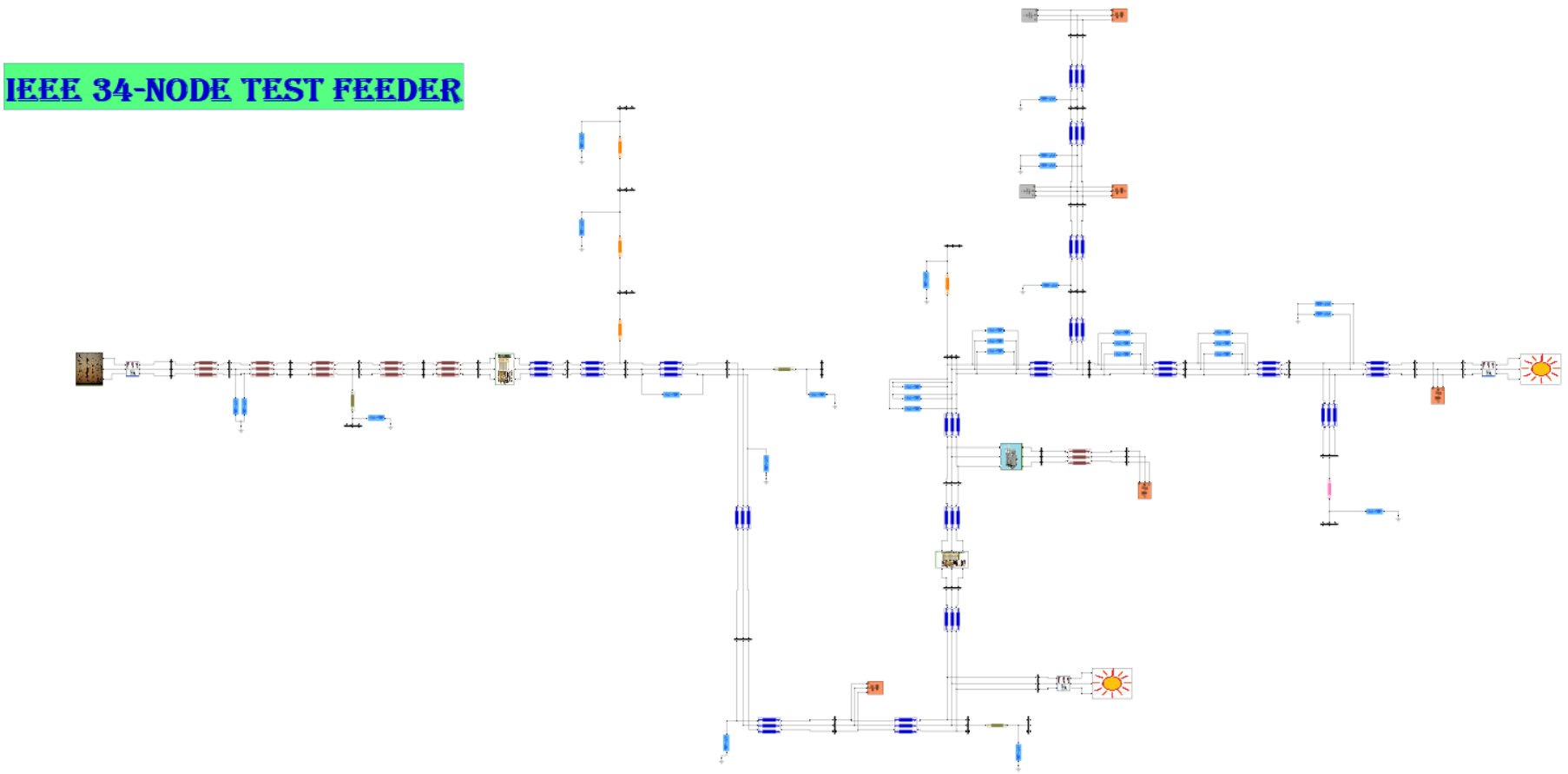

Figure 2.12: MATLAB™ model of IEEE 34-node distribution feeder

CHAPTER 3

DESIGNING THE DISTRIBUTED GENERATION – PV UNIT

- Overview
- Role of Solar Energy
- Maximum Power Point Tracking
- DC-DC Converter
- DC-AC Inverter System

3.1 OVERVIEW

The International Council on Large Electric Systems' (French: *Conseil International des Grands Réseaux Électriques*, *CIGRÉ*) CIGRÉ 6.2 sub-committee defines "Microgrids are electricity distribution systems containing loads and distributed energy resources, (such as distributed generators, storage devices, or controllable loads) that can be operated in a controlled, coordinated way either while connected to the main power network or while is landed."

The International Council on Large Electric Systems is a global organisation in the field of high voltage electricity founded in Paris in 1921. Working with the definition the focus is kept on the islanding of the microgrid in this work. Islanding is a condition defined when the DG is isolated from the main utility due to intentional or unintentional islanding and where the DG's are sufficient enough to feed all the loads connected to it. During this span power must be supplied to maintain the grid parameters and provide supply to the loads. In order to achieve this the microgrid must operate in an islanded mode efficiently for which planning and coordination is required.

While designing the microgrid the background scenario was kept on developing countries like India. Because of the geographic location it is situated on India gets an abundant amount of sunlight throughout the year which can be harnessed into energy and can be processed to feed microgrids acting as distributed generation sources. India, a rapidly growing economy with more than 1 billion people, is facing a huge energy demand. The country stands fifth in the world in the production and consumption of electricity. The electricity production has expanded over the years, but we cannot deny the fact that the population of the country is also expanding. The power produced in the country is mostly from coal (53%) and it is predicted that country's coal reserves won't last beyond

2040-50. More than 72% population living in villages and half of the villages remain without seamless supply of electricity. Also, the different sources of energy generation are distributed erratically which increases cost of transportation of energy to load sites. It's high time that focus should be made more on energy efficiency, conservation and renewable energy. To meet this surging demand, solar energy is the best form of energy to fulfil the energy needs of India and bridge the energy demand-supply gap [17].

There are ofcourse several advantages in maintaining a microgrid in a power system. The major of them being:

- Microgrids improve the energy delivery to local loads. This gives choice to switch between the most efficient source of energy available besides reducing carbon footprint and lowering energy generation costs.
- Microgrids ensures to satisfy uninterruptible power supply needs for emergency services in case of a system islanding.
- In distribution networks, a microgrid acts as a virtual power source or load. Therefore, peak shaving can be realized through coordinated control of distributed generation and loads.
- Microgrids integrate distributed and renewable energy resources to reduce peak load congestion and line losses by locating generation near demand.
- Microgrids require very low financial commitments and aids in economic growth.

The key feature that makes the microgrid possible is the power electronics, control, and communications capabilities that permit a microgrid to function as a semi-autonomous power system. The power electronics are the critical distinguishing feature of the microgrid as discussed in details hereafter. Renewable generation could appear in

microgrids, especially those interconnected through power electronic devices, such as photovoltaic systems. This enables power generation at distribution voltages. This enables control of the microgrid as single unit that meets the operation standards of the local utility. Microgrid is suitable for supplying power to the remote regions where supply from the grid is either difficult to avail or is not reliable due to severe geographic or weather conditions. The main grid treats microgrid as a single controllable entity which can be operated as a single aggregated load. This is important in ensuring reliability, security and compliance with the local utility standards. However, to achieve a stable and secure microgrid operation, several technical and economic issues needs are needed to be analysed.

Some of the attributes of microgrid are:-

- It is not centrally planned and dispatched.
- It is usually smaller than 50MW.
- Power is directly fed to the utility.
- Distributed energy resources are closer to the customers.

3.2 ROLE OF SOLAR ENERGY

The geographical location of tropical countries like India stands to its benefit for generating solar energy. The reason being solar radiation is being received almost throughout the year, which amounts to 3,000 hours of sunshine. This is equal to more than 5,000 trillion kWh with almost an average of 4-7 kWh of solar radiation per sq. metres. This is equivalent to 2,300–3,200 sunshine hours per year. Since majority of the population lives in rural areas in the tropical countries, there is much scope for solar energy being promoted in these areas. Use of solar energy can reduce

the use of firewood and dung cakes by rural household. States like Andhra Pradesh, Bihar, Gujarat, Haryana, Madhya Pradesh, Maharashtra, Orissa, Punjab, Rajasthan, and West Bengal in India have great potential for tapping solar energy due to their location.

Some of the advantages of solar energy which makes it more suitable are as follows:

i. This is an inexhaustible source of energy and the best replacement to other non-renewable energies.
ii. Solar energy is environment friendly. When in use, it does not release CO_2 and other gases which pollute the air. Hence it is very suitable for countries where pollution is a matter of grave concern.
iii. Solar energy can be used for variety of purposes like as heating, drying, cooking or electricity, which is suitable for the rural areas like in India. It can also be used in cars, planes, large power boats, satellites, calculators and many more such items, just apt for the urban population.
iv. Solar power is inexhaustible. In any energy deficient country, where power generation is costly, solar energy is the best alternate means of power generation.
v. A solar energy system can be installed anywhere. Solar panels can be easily placed in houses. Hence, it is quite inexpensive compared to other sources of energy.

3.3 MAXIMUM POWER POINT TRACKING (MPPT)

Typically, a solar cell can be modelled by a current source and an inverted diode connected in parallel to it. It has its own series and parallel resistance. Series resistance is due to hindrance in the path of flow of

electrons from n to p junction and parallel resistance is due to the leakage current.

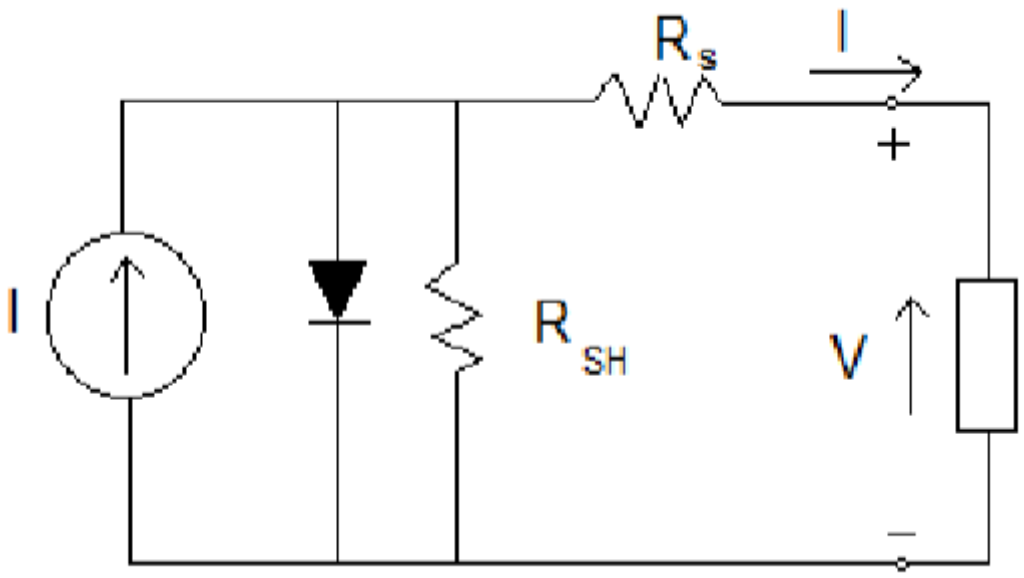

Figure 3.1: Single diode model of a PV cell

The single diode model of a PV cell [9] is shown in Figure 3.1, where current source (I) along with a diode and series resistance (Rs). The shunt resistance (RSH) in parallel is very high has a negligible effect and can be neglected. The output current from the photovoltaic array is

$$I = I_{sc} – I_d$$

$$I_d = I_o \left(e^{qV_d/kT} - 1\right)$$

Where, I_o is the reverse saturation current of the diode, q is the electron charge, V_d is the voltage across the diode, k is Boltzmann constant ($1.38 * 10^{-19}$ J/K) and T is the junction temperature in Kelvin (K). Hence,

$$I = I_{sc} – I_o \left(e^{qV_d/kT} – 1\right)$$

Using suitable approximations,

$$I = I_{sc} - I_o \left(e^{q((V+IRs)/nkT)} - 1\right)$$

where, I is the photovoltaic cell current, V is the PV cell voltage, T is the temperature (in Kelvin) and n is the diode ideality factor. In order to model the solar panel accurately we can use two diode model but in here study is limited to the single diode model. Also, the shunt resistance is very high and can be neglected during the course of our study.

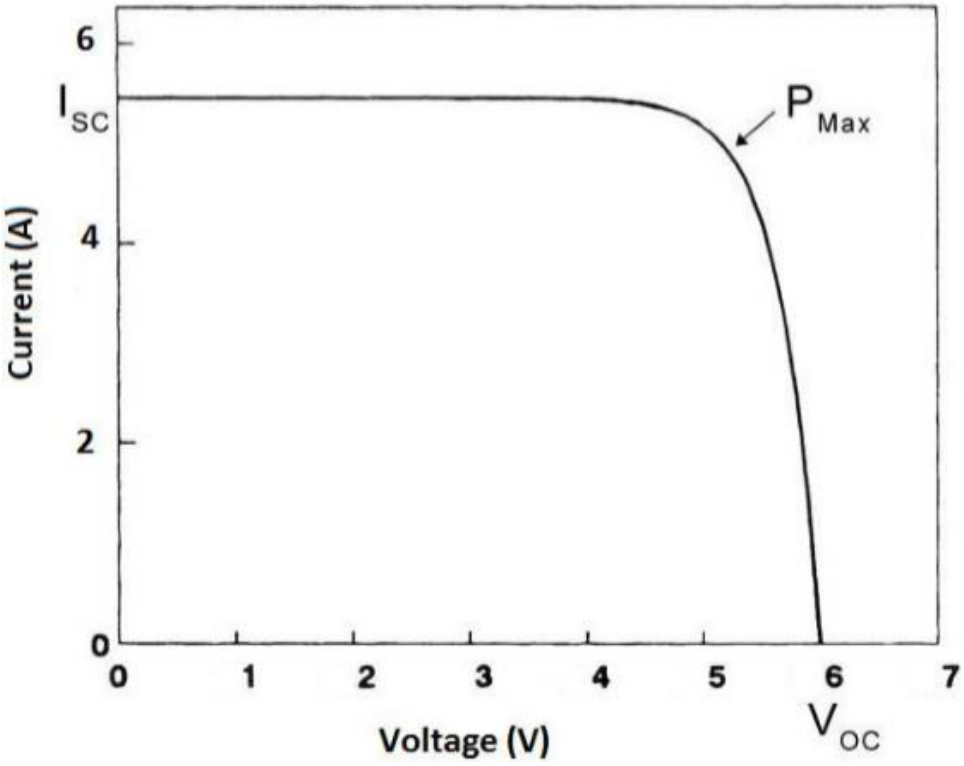

Figure 3.2: I-V characteristics of a solar panel

The I-V characteristics of a typical solar cell are as shown in the Figure 3.2. When the voltage and the current characteristics are multiplied, we get the P-V characteristics as shown in Figure 3.3. The point indicated as MPP is the point at which the panel power output is maximum.

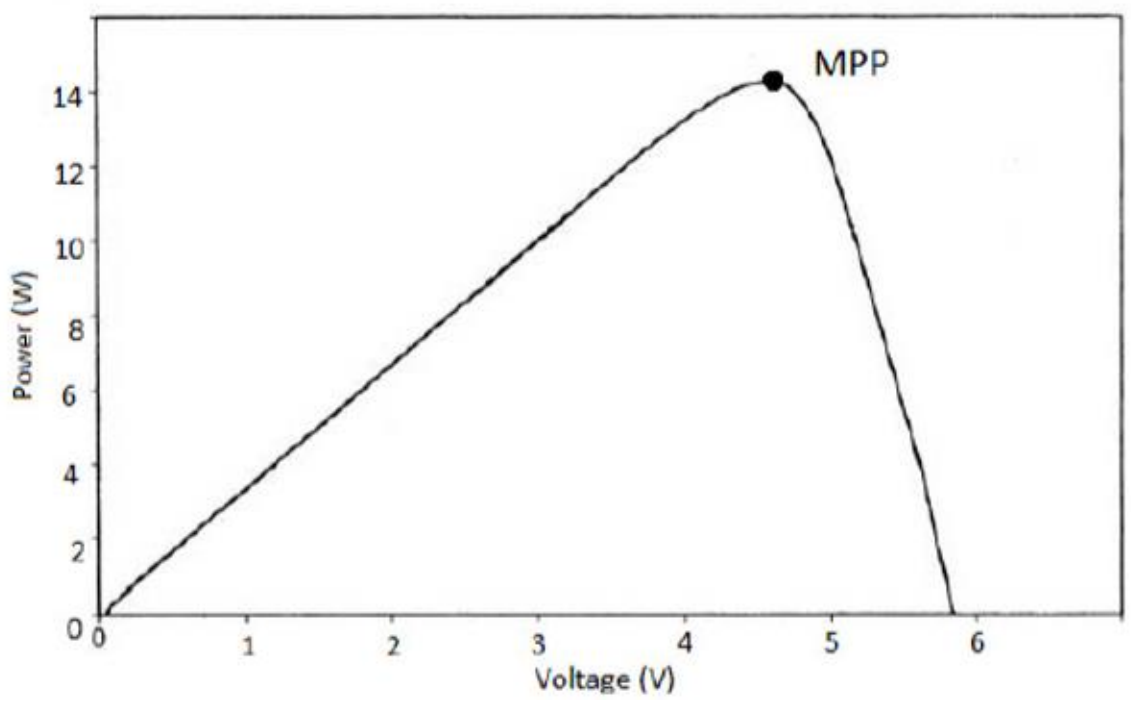

Figure 3.3: PV characteristics curve of a photovoltaic cell

Maximum power point tracking (MPPT) is a technique used commonly with wind turbines and photovoltaic (PV) solar systems to maximize power extraction under all conditions. Photovoltaic cells have a complex relationship between their operating environment and the maximum power they can produce. The fill factor, abbreviated *FF*, is a parameter which characterizes the non-linear electrical behaviour of the solar cell. Fill factor is defined as the ratio of the maximum power from the solar cell to the product of open circuit voltage V_{oc} and short-circuit current I_{sc}. In tabulated data it is often used to estimate the maximum power that a cell can provide with an optimal load under given conditions,

$$P = FF * V_{oc} * I_{sc}$$

For most purposes, FF, V_{oc}, and I_{sc} are enough information to give a useful approximate model of the electrical behaviour of a photovoltaic cell under typical conditions. For any given set of operational conditions, cells have a single operating point where the values of the current (*I*) and

voltage (*V*) of the cell result in a maximum power output. These values correspond to a particular load resistance, which is equal to *V* / I as specified by Ohm's Law. The power P is given by,

$$P = V * I$$

A photovoltaic cell, for the majority of its useful curve, acts as a constant current source. [10] However, at a photovoltaic cell's maximum power point region, its curve has an approximately inverse exponential relationship between current and voltage.

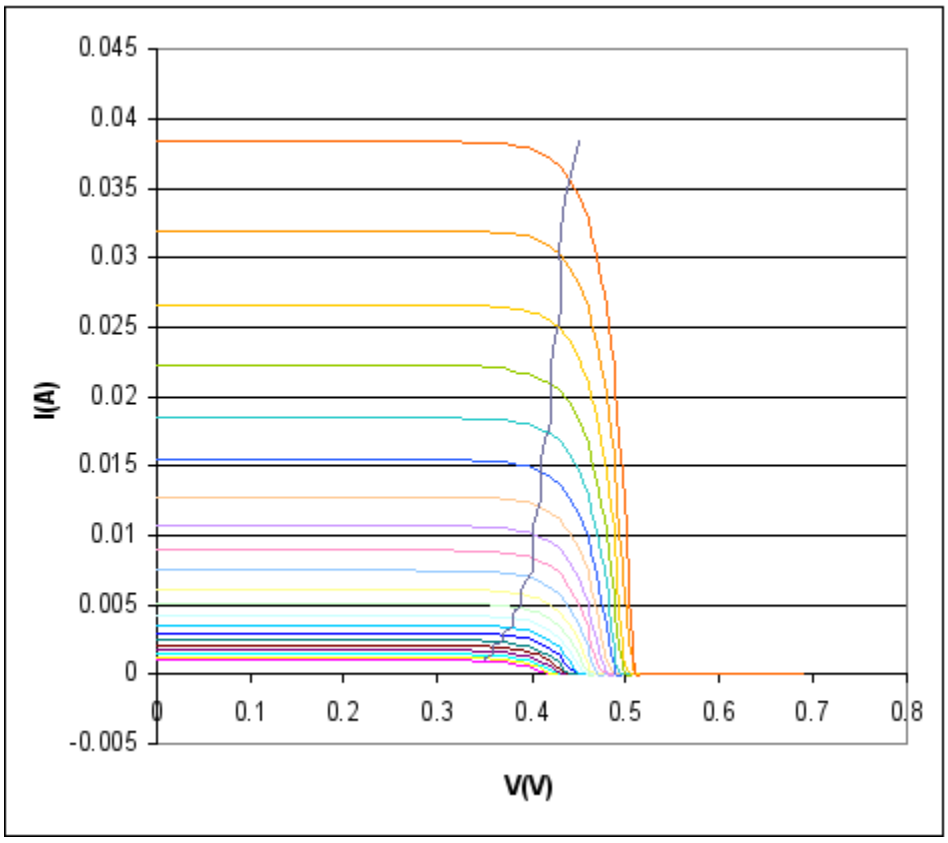

Figure 3.4: Solar cell I-V curve in varying sunlight

From basic circuit theory, the power delivered from or to a device is optimized where the derivative (graphically, the slope) $\frac{dI}{dV}$ of the I-V curve is equal and opposite the *I/V* ratio (where $\frac{dP}{dV} = 0$). This is known as the *maximum power point* (MPP) and corresponds to the "knee" of the curve. Figure 3.4 shows the solar cell curve in varying sunlight. Photovoltaic solar

cell I-V curves where a line intersects the “knee” of the curves where the maximum power transfer point is located.

A load with resistance $R=V/I$ equal to the reciprocal of this value draws the maximum power from the device. This is sometimes called the 'characteristic resistance' of the cell. This is a dynamic quantity which changes depending on the level of illumination, as well as other factors such as temperature and the age of the cell. If the resistance is lower or higher than this value, the power drawn will be less than the maximum available, and thus the cell will not be used as efficiently as it could be. Maximum power point trackers utilize different types of control circuit or logic to search for this point and thus to allow the converter circuit to extract the maximum power available from a cell.

When a load is directly connected to the solar panel, the operating point of the panel will rarely be at peak power. The impedance seen by the panel derives the operating point of the solar panel. Thus, by varying the impedance seen by the panel, the operating point can be moved towards peak power point. Since panels are DC devices, DC-DC converters must be utilized to transform the impedance of one circuit (source) to the other circuit (load). Changing the duty ratio of the DC-DC converter results in an impedance change as seen by the panel. At a particular impedance (i.e. duty ratio) the operating point will be at the peak power transfer point. The I-V curve of the panel can vary considerably with variation in atmospheric conditions such as radiance and temperature. Therefore, it is not feasible to fix the duty ratio with such dynamically changing operating conditions. MPPT implementations utilize algorithms that frequently sample panel voltages and currents, then adjust the duty ratio as needed with the help of a controller.

The different methods of MPPT operations are:

- Perturb and observe
- Incremental conductance
- Current sweep
- Constant voltage
- Temperature Method

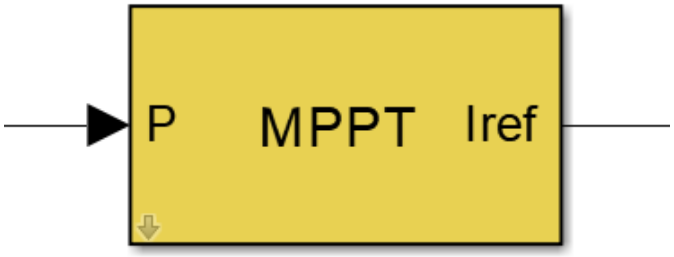

Figure 3.5: Custom Simulink™ model for MPPT block

In this work, the method of perturb and observe is being used. In this method the controller adjusts the voltage by a small amount from the solar array and measures power; if the power increases, further adjustments in that direction are tried until power no longer increases. This is called the perturb and observe method and is most common, although this method can result in oscillations of power output. It is referred to as a hill climbing method, because it depends on the rise of the curve of power against voltage below the maximum power point, and the fall above that point. Perturb and observe is the most commonly used MPPT method due to its ease of implementation. Perturb and observe method may result in top-level efficiency, provided that a proper predictive and adaptive hill climbing strategy is adopted.

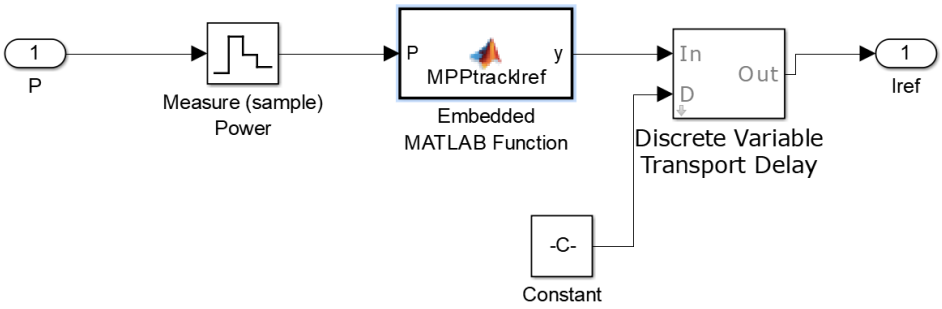

Figure 3.6: Internal design of MPPT block

The code shown in Appendix A.4 for the 'perturb and observe' method block enforces the algorithm for the microgrid.

3.4 DC-DC CONVERTER

In the previous unit, it was mentioned that since we are working with DC devices, DC-DC converters must be used. The PV system produces voltages in the order of few hundreds of volts. But in order to match the voltage of the existing grid it has to be stepped up at first. In order to apply this concept in our system, a DC-DC converter has been introduced which works on the principle of current mode control. Current mode control is a two-loop system. The switching power supply inductor is "hidden" within the inner current control loop. This simplifies the design of the outer voltage control loop and improves power supply performance in many ways, including better dynamics. The objective of this inner loop is to control the state-space averaged inductor current, but in practice the instantaneous peak inductor current is the basis for control. (Switch current --equal to inductor current during the "on" time--is often sensed.) If the inductor ripple current is small, peak inductor current control is nearly equivalent to average inductor current control. In a conventional switching power supply employing a buck derived topology, the inductor is in the output. Current mode control then, is actually, output current control,

resulting in many performance advantages. On the other hand, in a high power factor pre-regulator using the boost topology, the inductor is in the input. Current mode control then controls input current, allowing it to be easily conformed to the desired sinusoidal waveshape.

But, along with it there are several drawbacks in using peak current mode control. Majority among them being:

- The peak method of inductor current control functions by comparing the upslope of inductor current to a current program level set by the outer loop. The comparator turns the power switch off when the instantaneous current reaches the desired level. The current ramp is usually quite small compared to the programming level, especially when V_{IN} is low. As a result, this method is extremely susceptible to noise. A noise spike is generated each time the switch turns on. A fraction of a volt coupled into the control circuit can cause it to turn off immediately, resulting in a subharmonic operating mode with much greater ripple. Circuit layout and bypassing are critically important to successful operation.
- The peak current mode control method is inherently unstable at duty ratios exceeding 0.5, resulting in sub-harmonic oscillation. A compensating ramp (with slope equal to the inductor current downslope) is usually applied to the comparator input to eliminate this instability. In a buck regulator the inductor current downslope equals V_o/L. With V_o constant, as it usually is, the compensating ramp is fixed and easy to calculate-but it does complicate the design. With a boost regulator in a high power factor application, the downslope of inductor current equals $(V_{IN}-V_o)/L$ and thus varies considerably as the input voltage follows the rectified sine waveform. A fixed ramp providing adequate compensation will

overcompensate much of the time, with resulting performance degradation and increased distortion.

- The peak to average current error inherent in the peak method of inductor current control is usually not a serious problem in conventional buck derived power supplies. This is because inductor ripple current is usually much smaller than the average full load inductor current, and because the outer voltage control loop soon eliminates this error. In high power factor boost pre-regulators the peak/avg error is very serious because it causes distortion of the input current waveform. While the peak current follows the desired sine wave current program, the average current does not. The peak/avg error becomes much worse at lower current levels, especially when the inductor current becomes discontinuous as the sine wave approaches zero every half cycle. To achieve low distortion, the peak/avg error must be small. This requires a large inductor to make the ripple current small. The resulting shallow inductor current ramp makes the already poor noise immunity much worse.

So, therefore the average current mode control is used in the control of the DC-DC boost converter. Peak current mode control operates by directly comparing the actual inductor current waveform to the current program level at the two inputs of the PWM comparator. This current loop has low gain and so cannot correct for the deficiencies noted above.

The technique of average current mode control [11] overcomes these problems by introducing a high gain integrating current error amplifier (CA) into the current loop. A voltage across R_p, (set by the outer loop) represents the desired current program level. The voltage across current sense resistor R_s, represents actual inductor current. The

difference, or current error, is amplified and compared to a large amplitude sawtooth (oscillator ramp) at the PWM comparator inputs. The gain-bandwidth characteristic of the current loop can be tailored for optimum performance by the compensation network around the CA. Compared with peak current mode control, the current loop gain crossover frequency, f_c , can be made approximately the same, but the gain will be much greater at lower frequencies [12] as demonstrated in Figure 3.7.

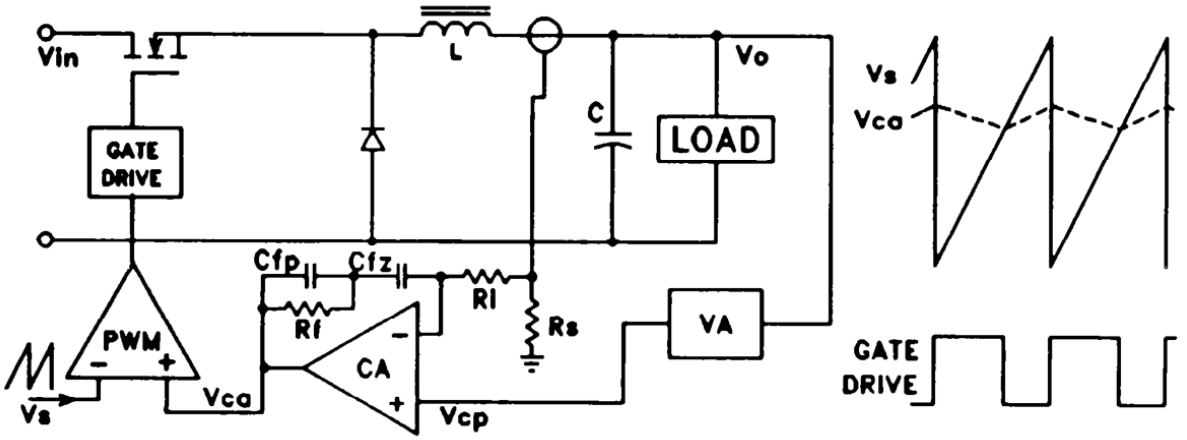

Figure 3.7: Average current control mode circuit and waveforms

The result is:

- Average current tracks the current program with a high degree of accuracy. This is especially important in high power factor pre-regulators, enabling less than 3% harmonic distortion to be achieved with a relatively small inductor. In fact, average current mode control functions well even when the mode boundary is crossed into the discontinuous mode at low current levels. The outer voltage control loop is oblivious to this mode change.
- Slope compensation is not required, but there is a limit to loop gain at the switching frequency in order to achieve stability.
- Noise immunity is excellent. When the clock pulse turns the power switch on, the oscillator ramp immediately dives to its lowest level,

volts away from the corresponding current error level at the input of the PWM comparator.

- The average current mode method can be used to sense and control the current in any circuit branch. Thus, it can control input current accurately with buck and flyback topologies and can control output current with boost and flyback topologies.

The design implemented in this work uses this average current mode control. The system of average current control mode was made possible by Simulink™ blocks as shown in Figure 3.8 where resemblance is found with Figure 3.7.

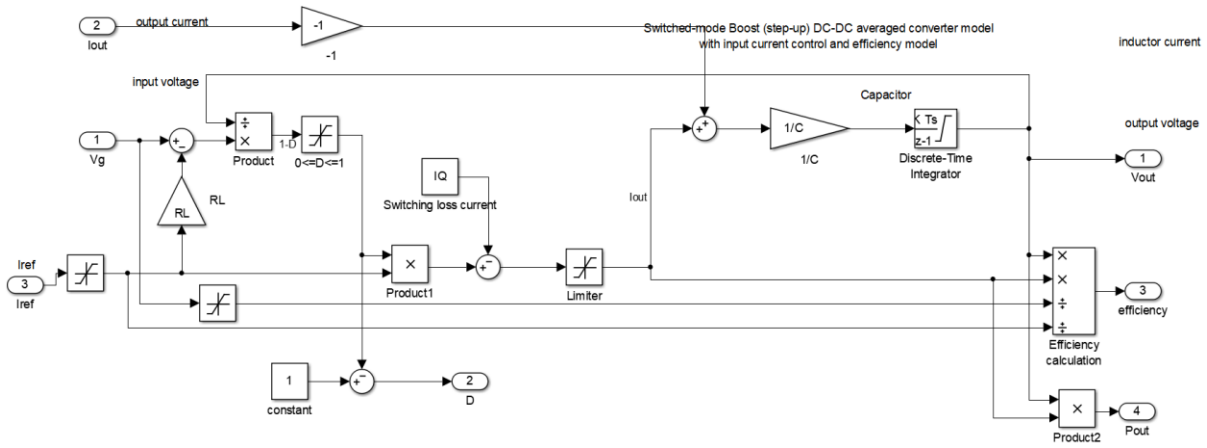

Figure 3.8: Simulink™ model of average current mode control

3.5 DC-AC INVERTER SYSTEM

In implementation of the conversion system from dc-ac values of voltage or current in the voltage source inverter, the switched mode of the inverter is used generally. [13] A wide range of power conversion applications use the current control technique. This technique controls the peak inductor current to regulate the converter output. The most drawbacks of current control are a poor noise immunity and instability at duty ratios exceeding 0.5. That is a robust structure which results in usable output across its outputs. Although the switched mode inverter

model is useful for a physical inverter, it is nonlinear because of the switching. The output voltage obtained rises in considerable steps and does not produce a smooth waveform required for use in the microgrid. Because of this a linear model is designed in order to obtain a frequency characteristic which can be easily studied. The average mode control is a control technique that overcomes problems listed above. Average mode of control is a two-loop technique that uses an integrator in the inner loop to average the sensed current. That is why in this work the inverter is used as an average mode model. Also, the time required for simulating an average model is significantly lowered compared to the switched model because the simulation size step can be increased (the frequency of the switching doesn't appear in the average model). The average model is the ideal model for designing and developing control systems.

The inverters must function with or without load (light) or no-load. The conditions categorize into two different cases. First, the power utilized by the load decreases to zero, second, in the event that a malfunction occurs at the output, the inverter will have to work empty. Whatever the reason of the drop of the load, the inverter must be functional. [14]

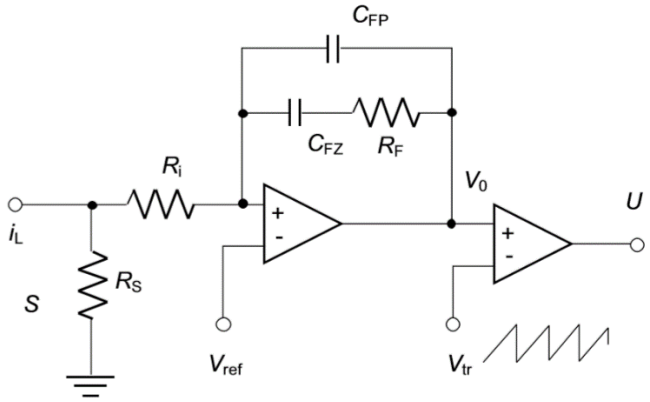

Figure 3.9: Average mode of control of voltage source inverter schematics

A circuit scheme that could be used to implement ACMC is shown in Figure 3.9. The current to be controlled is sensed through R_S and

averaged. The voltage reference V_{ref} is delivered by the outer loop. The integrator output is compared to a triangular waveform, the switch control is then generated. The transfer function of the integrator circuit is described below.

$$V_0 = V_{ref} + (V_{ref} - V_i) [(sR_FC_{FZ} + 1) / sR_i . (sR_F . C_{FP.FZ} + C_{FP} + C_{FZ})]$$

where $V_i = R_S \cdot i_L$.

So, the algorithm is used to implement it in Simulink™ environment which is shown in the Figure 3.10.

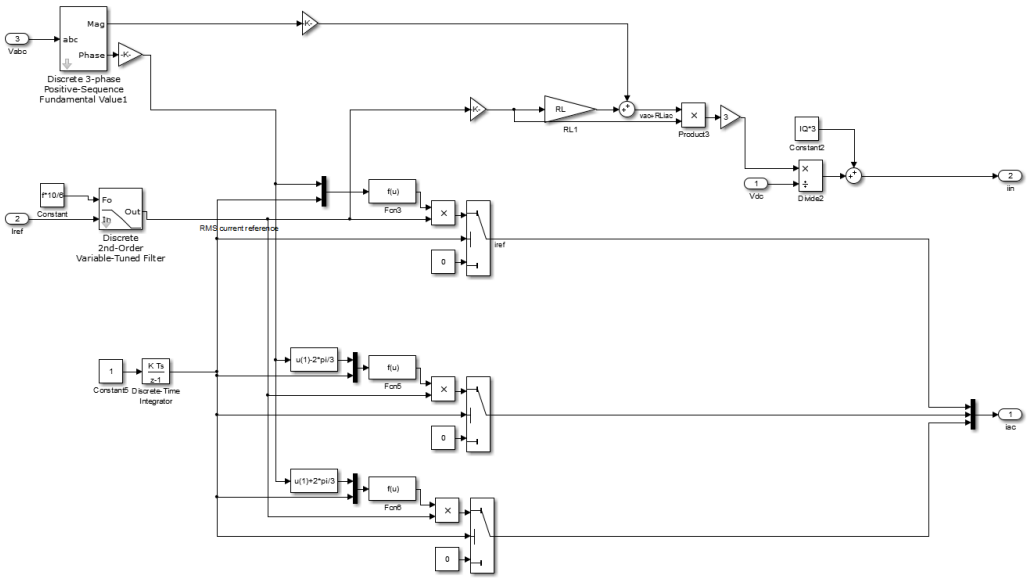

Figure 3.10: Simulink™ model for averaged mode model of inverter

The current outputs for the three phases are then separated using a demux block in Simulink™. The currents are measured and regulated as seen in Figure 3.11. To receive the bus voltage requirement at the output, the currents from the three phases are passed through the three resistances in the respective phase whose values are set as per voltage requirement calculations, output power rating of the microgrid and impedance matching with the grid. The voltage calculations for the three phase - red, yellow and blue, are made with respect to the ground as seen.

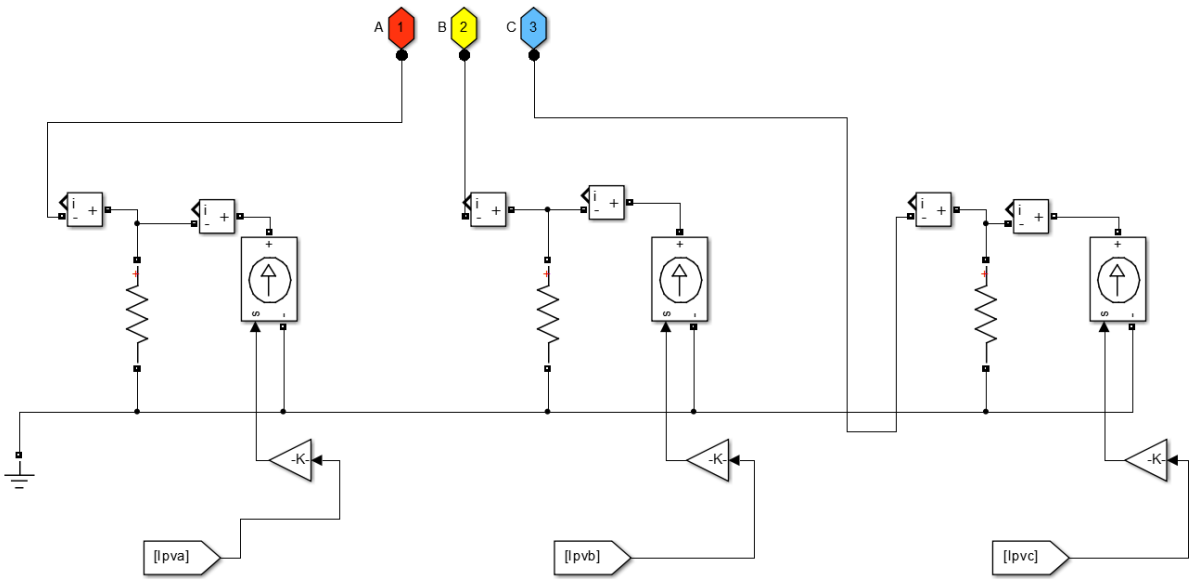

Figure 3.11: Voltage setting at output terminals of microgrid

CHAPTER 4

REAL-TIME MODELING IN OPAL-RT™

- Introduction
- Hardware and Software Requirements for Modelling and Simulation
- Time selection setting in OPAL-RT™ & RT-LAB™
- Modelling in RT-LAB™

4.1 INTRODUCTION

A discrete-time constant step duration simulation is assumed for discussion in this work. Discrete time simulation means that time moves forward in fixed step size, which is also known as fixed time step simulation. Even though there are some methods and simulation such as variable step solver in Simulink™ , which use variable step size for solving high frequency dynamics, they are unsuitable for real-time simulation.

That is why we use the tools available to us for real time simulations: OPAL-RT™ and RT-LAB™. RT-LAB™ is OPAL-RT™ 's real-time simulation software combining performance and enhanced user experience. Fully integrated with MATLAB/Simulink™, RT-LAB™ offers the most complex model-based design for interaction with real-world environments. It provides the flexibility and scalability to achieve the most complex real-time simulation applications in the automotive, aerospace, power electronics, and power systems industries.

Since its first application nearly 20 years ago on the Canadian Space Agency's Canada Arm, RT-LAB has revolutionized the world of systems engineering, whether in space, on the ground or at sea. RT-LAB enables engineers and scientists to accelerate the development of new prototypes and to meet the most rigorous testing required by new and innovative technologies.

4.2 HARDWARE AND SOFTWARE REQUIREMENTS FOR MODELLING AND SIMULATION

The hardware and the software requirements for real-time modelling and simulation in this work is as given below:

Hardware	Software
OPAL-RT™ OP5600	Host operating system: Windows 10™
	Target operating system: Redhat™
	RT-LAB™ v11.0
	MATLAB™ v2013a
	Simulink™ v8.1

Table 4.1: Software and Hardware specifications of real-time simulation

4.3 TIME SELECTION SETTING IN OPAL-RT™ & RT-LAB™

A real-time simulation bases its calculation and solving processes not only on the computational speed of the hardware but also on the complexity of the model designed. A real-time simulator produces results at within the same domain and measurements as its real-world physical model would produce. The step time that is provided to it is required not just for computing the mathematical models, but it also is the essential time information to drive the input and output ports. The concern regarding time setting is the problem regarding overrun and excess idle time. There will be loss in the form of idle time if the computation is completed before the step time is reached. Also, if the computation takes time more than the step time then there will be minor to acute data loss. Such an example is cited in the Figure 4.1.

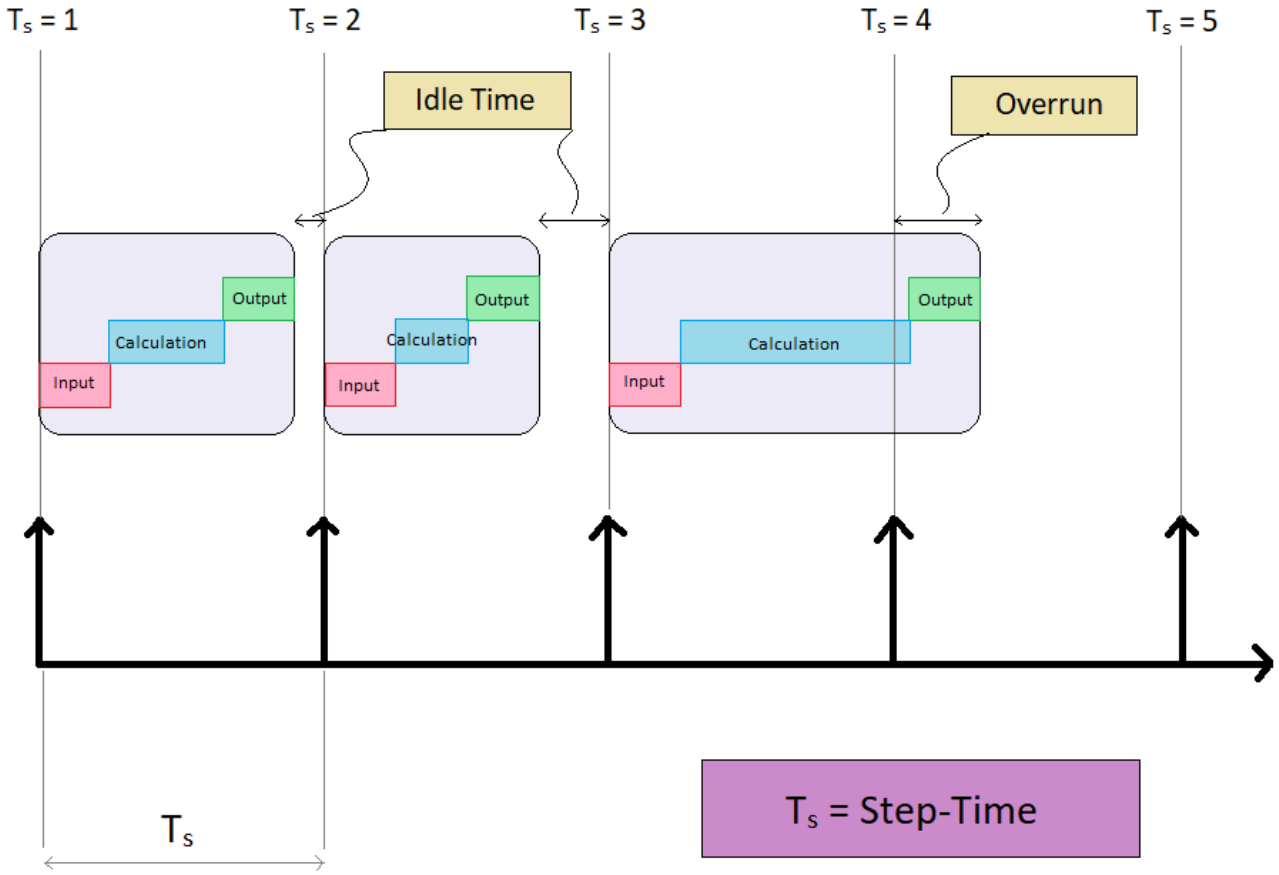

Figure 4.1: Step time mechanism for RT-LAB™

As seen in the Figure 4.1, for step time series of 1 second, in the first two case, the idle time is in acceptable range and in the next one it is quite measurable. This must be avoided because during this period the system's computational resources are not utilised and it adds to the apparent computation time of the system. In the second case it is seen that the total computation time exceeds the step time period and, in this case, data is lost. This is a more severe problem than enlarged idle time because due to loss of system data the results obtained will be erroneous. So, that's why idle time elongation and step time overrun should be avoided in real-time computation time settings. Keeping this in mind, the step-time of the computation is kept as T_s = 50 µs, which renders the model feasible for both Simulink™ & RT-LAB™ environments.

4.4 MODELLING IN RT-LAB™

RT-LAB™ is a real-time simulation platform for high-fidelity plant simulation, control system prototyping, and embedded data acquisition and control. The unique distributed processing capability of RT-LAB™ allows to convert the Simulink™ models to high-speed, real-time simulations, over one or more target PC processors.

RT-LAB™ enables models in Simulink™ environment models to interact with real world objects enabling the hardware-in-loop(HIL) engineering simulators. RT-LAB™ links the code generated with Simulink™ coder to optimized runtime libraries for compatibility in physical world. This helps to achieve an irregularity-free fixed step. RT-LAB™ automates the process of preparation, downloading and running of parallel models in the system. There are two parts of OPAL-RT™ simulator; the command station and the target node.

Command station is described as a Windows™ PC with RT-LAB™ software servers as the development system and user interface. It allows the user to create and prepare the model for distributed real-time execution and interaction during run-time. Target node is a cluster of PCs where the simulator runs. For simulating in real-time, a Real-Time Operating System (RTOS) such as RedHat™ Real-Time Linux is required. The command station communicates with the target using Ethernet. For HIL simulations, the target communicates with the real world through I/O boards. Each target node can contain one or two processors and each processor can contain one, two, four, or six processor cores.

RT model consists of three type of subsystem in the topmost level. A Simulink™ model can be converted into RT-LAB™ compatible model with following changes also as referred by Figure 4.2:

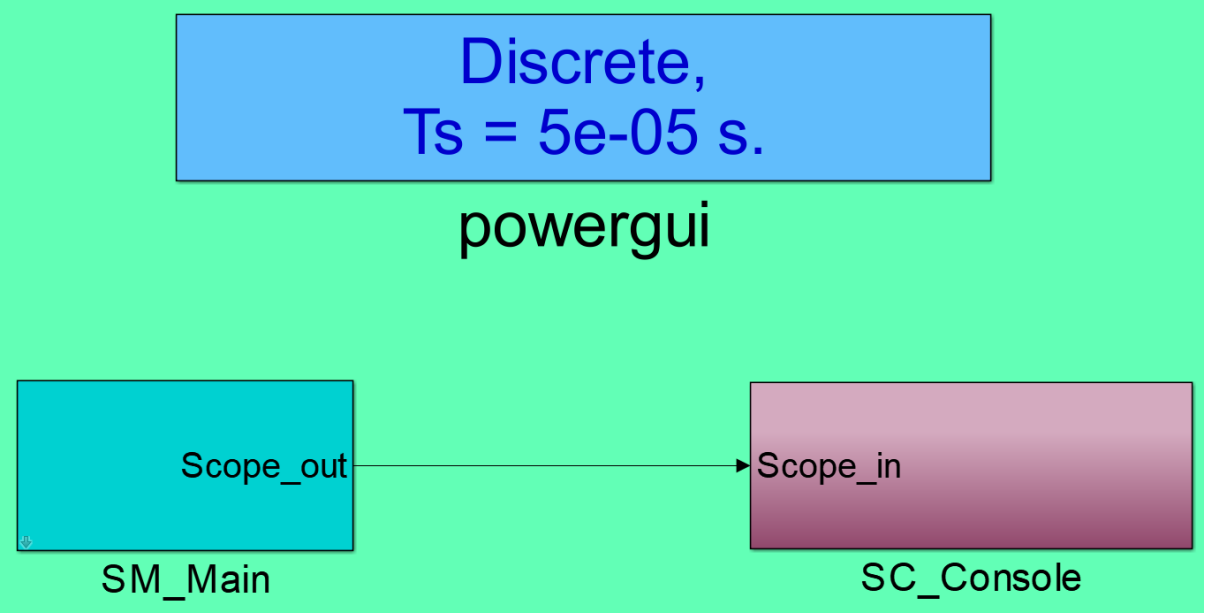

Figure 4.2: Simulink™ model compatible for RT-LAB™

- The POWERGUI™ block is placed at the topmost level of the model.
- All the scopes are placed in the console subsystem and all the other computational model in the Main/Master subsystem.
- The OpComm™ block [7] is used for communication between the subsystems as shown in Figure 4.3. All input ports must go through this block before it is connected inside the subsystem.

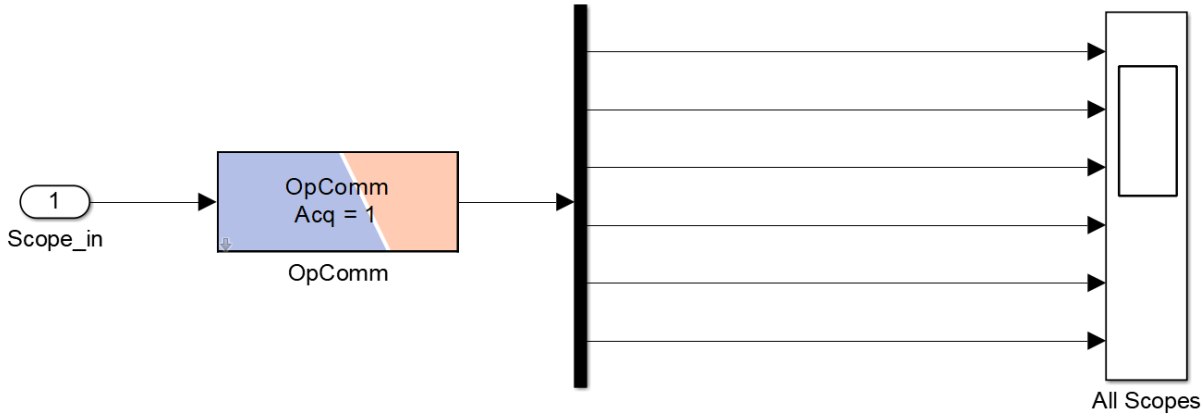

Figure 4.3: OpComm™ block used as a communication tool

The observations recorded from the simulations were recorded and studied which are being discussed in the following chapter.

CHAPTER 5

SIMULATION & RESULTS

- Setting the simulation parameters
- Simulation results

5.1 SETTING THE SIMULATION PARAMETERS

As discussed in the previous chapter, special attention was needed to be taken while setting the simulation step-time for the computation of the model. It is known that a larger step time reduces calculation complexity and computation resources used but the accuracy of the output is also reduced with it. Because it is known that law relating computation time is inversely proportional to the computation resources used for a particular computation as shown by the Figure 5.1.

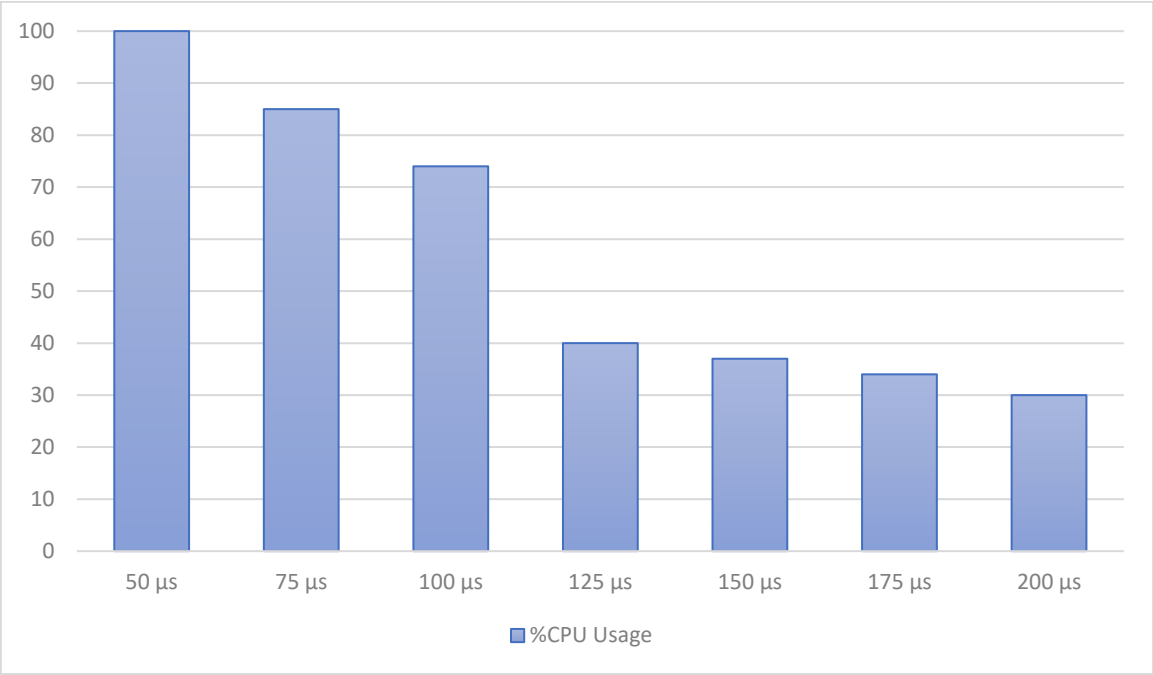

Figure 5.1: Percentage CPU usage with varying step-time for 34-node feeder

But the advantage with a shorter step time is that the results obtained has higher accuracy. Even though the computation time increases but it yields accurate results. Step sizes lesser than 50 µs was used as test which resulted in abnormally long durations of simulations and in few cases breakdown in the simulation process in the form of errors. That is why the step size of the simulation was set as T_s = 50 µs.

In the Simulink™ model configuration parameters settings, the following conditions are set:

- Solver type: Fixed-step
- Solver options: ode4 (Runge-Kutta)
- Fixed-step size (fundamental sample time): 50 µs
- Periodic sample time constraint: Unconstrained
- Tasking mode for periodic sample times: Auto

It is taken care of that the signal for the number of scopes combined via the mux block from the Main subsystem should have same configuration in the Console subsystem released via the demux block i.e. number of scopes on each side should be same. The value is set in the OpComm™ in the model. If not, there will be configuration errors.

It was decided that calculations will be taken in per unit (pu) values, so as reference the base voltage and base power were taken as:

$$V_{base} = 24.9 \text{ kV}$$

$$S_{base} = 500 \text{ kVA}$$

With the above-mentioned settings, the simulation is run from t = 0 secs. to t = 0.3 secs.

5.2 SIMULATION RESULTS

Since the IEEE 34 node radial distribution feeder is a very long feeder, we wanted to see the effects of islanding condition on the system and majorly two sets of observations:

i) If the voltage profile across the loads is sufficient as per rating.

ii) If the power supply is ample to supply for the load drops through the feeder.

Measurements were taken across four nos. of nodes viz. node-840, node-842, node-832, node-820 and node-800. In the simulations performed, the islanding occurred at t = 0.1 secs. and the whole system was disconnected from the main grid. The feeder was switched on to the PV at t = 0.2 secs. and hence observations were made in this case to study the feasibility of the DG systems in providing the above-mentioned requirements.

It is to be mentioned that the placements of the two nos. of DG units were not made in accordance to any algorithm. By observation and few trials undergone regarding the distribution of the load throughout the feeder, one no. of DG unit of 532 kW capacity was placed at the extreme sag end at node-840 as shown in Figure 5.2 and the other DG unit of 610 kW capacity was placed between node-852 and node-854 as shown in Figure 5.3.

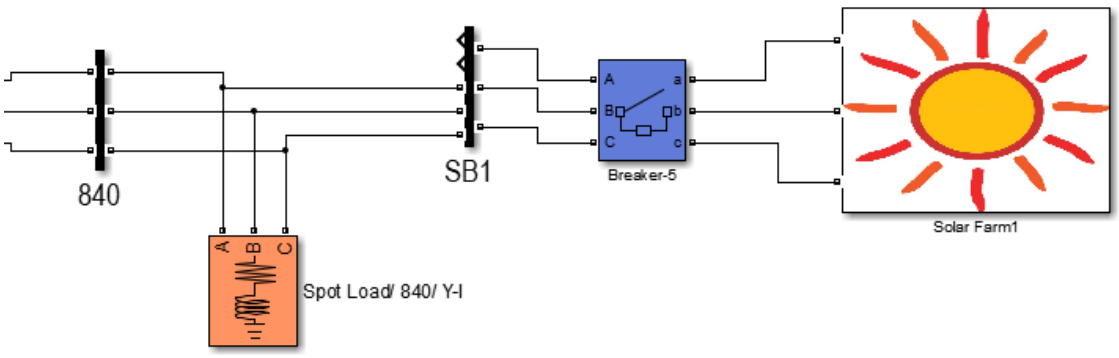

Figure 5.2: First PV unit DG system connected at node-840

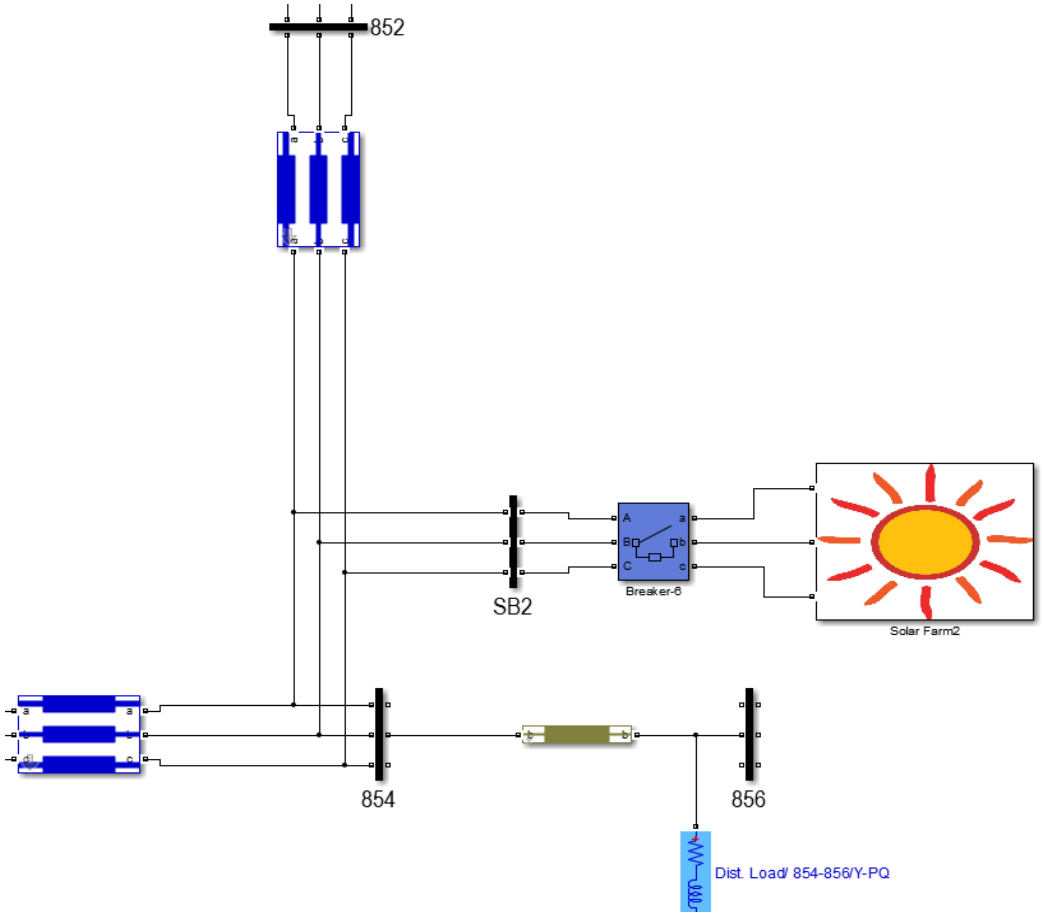

Figure 5.3: Second PV unit DG system connected between node-852 and node-854

Node-800

Initially, the main grid was connected at this node and so the voltage profile was the best maintained at this node. Although no load was attached to this node, this node served as the main connectivity to the rest of the grid. Due to the lengthy nature of the feeder, it is certain that there would be substantiable amount of the voltage drop through it. So, the voltage set at the node was about 4.5% higher than the nominal voltage for the feeder i.e. 24.9 kV, so that the voltage profile requirement is maintained till the sag end. After the islanding has occurred, the DG units were switched in. The voltage profile so obtained was 4.3% lower than the nominal voltage level which was within the acceptable range of the voltage requirements. Since, this node is situated about 41.24 km from the nearest DG unit, maintaining this voltage profile would be healthy in the

interlaying nodes. The current values die down to zero since no loads are attached to this node and after t = 0.1 secs. the grid is no more connected to this node. The voltage and current profile for this node is as shown in Figure 5.4.

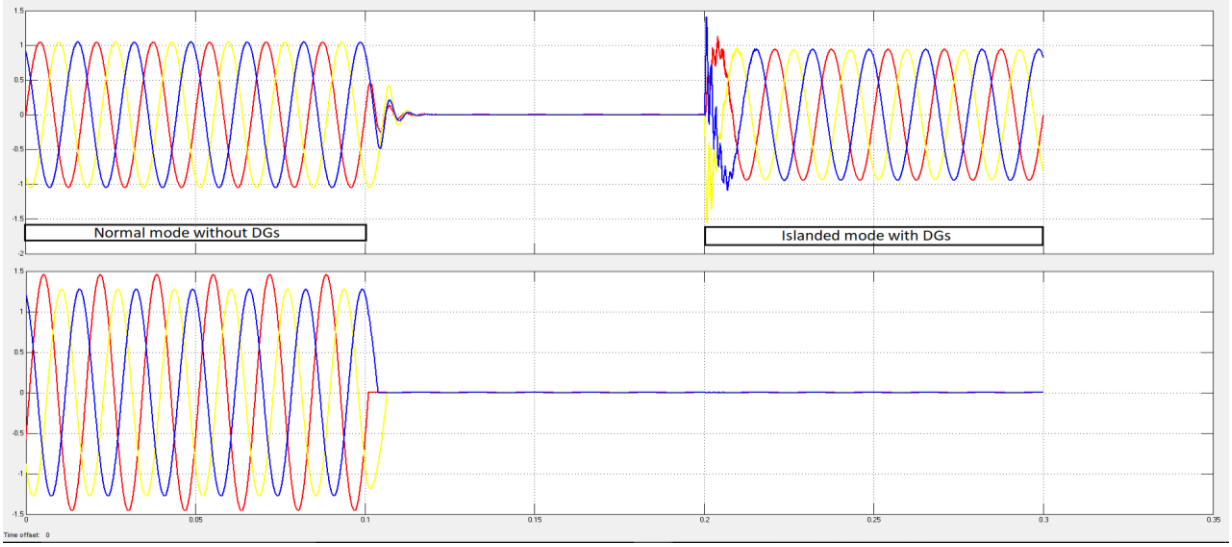

Figure 5.4: Voltage and Current waveforms of node-800 without and with the DGs

Node-820

The IEEE 34-node feeder contains both three phase loads and single-phase loads. Due to the differentiated distribution of loads throughout it is also noted that the single-phase loads are equally supplied as the other loads. Node-820 is such a node which is connected to a single-phase load at phase-B. Before the islanding occurs the voltage at this node is 1.126 pu and after the islanding while it is fed from the DG units the voltage is 1.1624 pu as shown in Figure 5.5. So, not only the voltage profile is satisfied but it is also improved in this case. The load attached to it was drawing powers 9.25 kW and 4.62 kVAr respectively. After it is fed from the DGs, the power levels are 9.74 kW and 4.87 kVAr respectively as shown in Figure 5.6. So, it is clear that the power requirements and the drops incurred are also satisfied at this node.

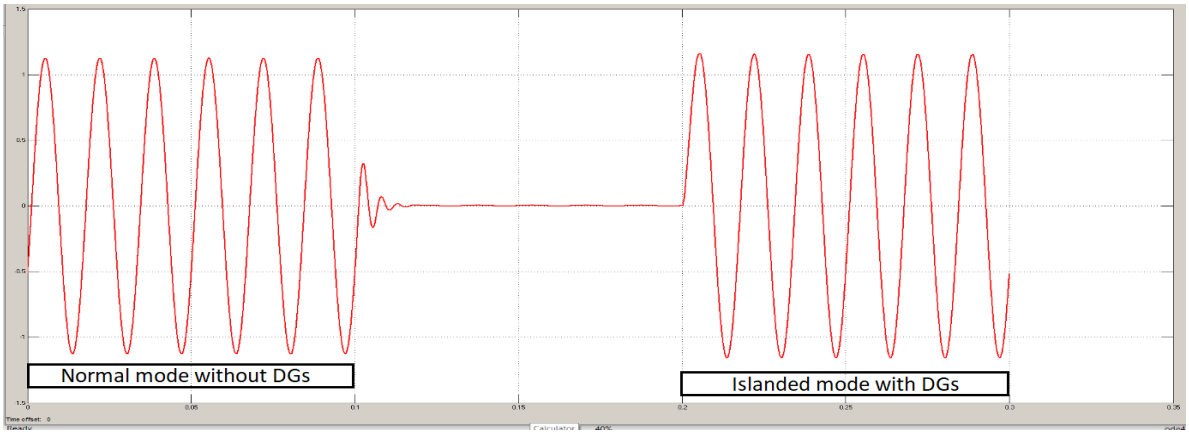

Figure 5.5: Voltage waveform of node-820 without and with the DGs

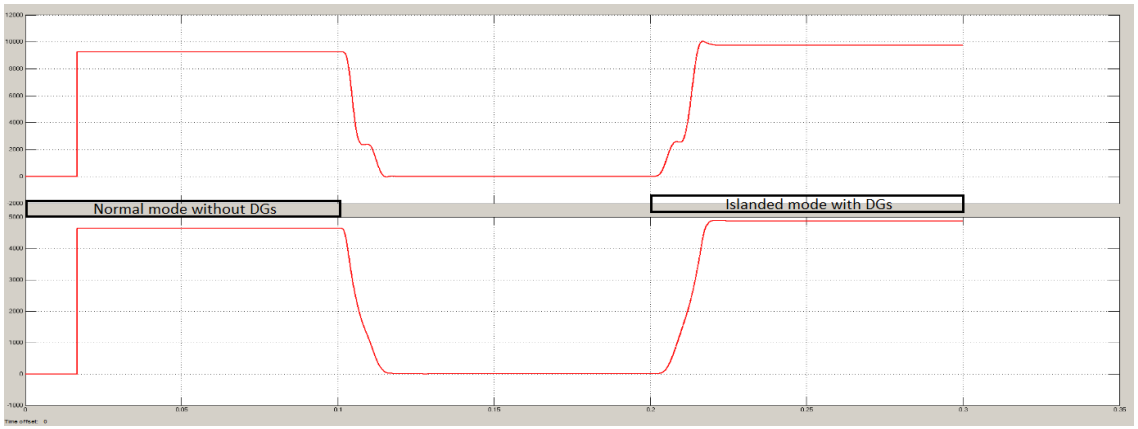

Figure 5.6: Active and Reactive power levels of node-820 without and with the DGs

Node-832

This node is a point of interest since it is located near XFM-1 i.e. a transformer which is a source of high magnetisation. So, maintaining the voltage profile was of utmost importance. Also, due to uneven loading in the three phases, the voltage amplitudes vary from one another. Say, taking phase-C as a point of study, before the DGs were introduced, the voltage was 0.8461 pu. After the islanding, with the DGs the voltage level observed was 0.86 pu as shown in Figure 5.7. So, the voltage profile was highly improved. While the DGs were not in the system, it was serving a power flow of 446.61 kW and 244 kVAr respectively. With only the DGs, the power flow was improved to 464.47 kW and 247.06 kVAr respectively as shown in Figure 5.8.

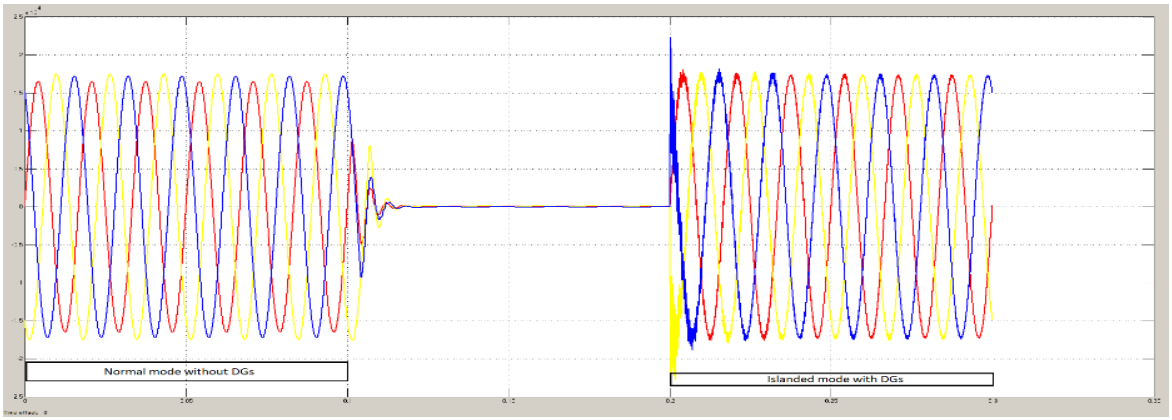

Figure 5.7: Voltage waveform of node-832 without and with the DGs

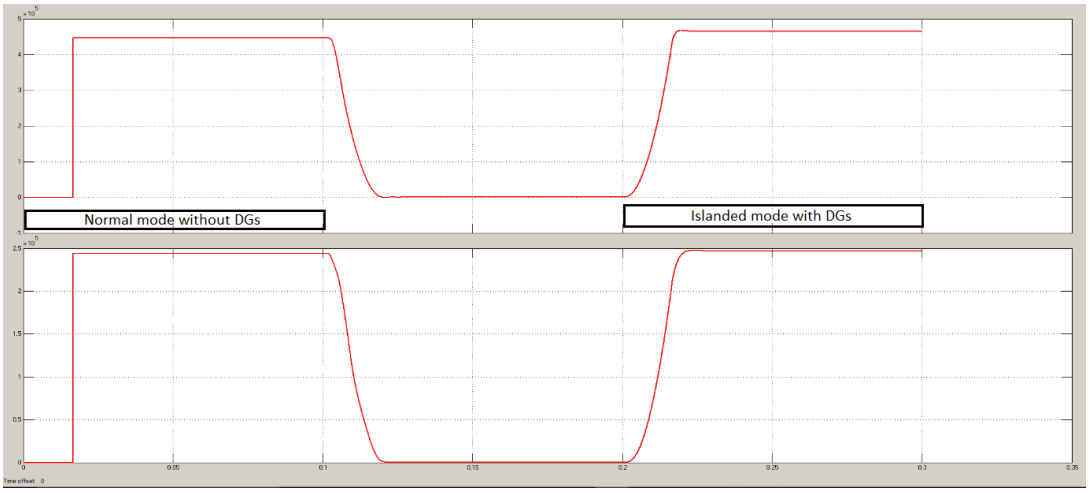

Figure 5.8: Active and Reactive power levels of node-832 without and with the DGs

Node-842

This node is taken to study the loads in the lateral branch of the feeder. It is closely situated to the sag end and in this region the feeder is heavily loaded. Taking reference with phase-B, the voltage profile at this node without DGs is 0.8582 pu. When the feeder is fed by the DGs only, the voltage is 0.8587 pu at the node as shown in Figure 5.9. This shows that the voltage profile is well maintained even if the feeder in this region is heavily loaded and prone to considerable voltage drop. In this branch, before the DGs were switched on, the power flow through the node was 126.4 kW and 90.457 kVAr respectively. Once the feeder was on the DGs only the power flow was 130.8 kW and 93.611 kVAr respectively as shown in Figure 5.10. also, the capacitor banks attached to in this branch helped

in maintaining the voltage profile. Thus, the power supply to the loads are well maintained.

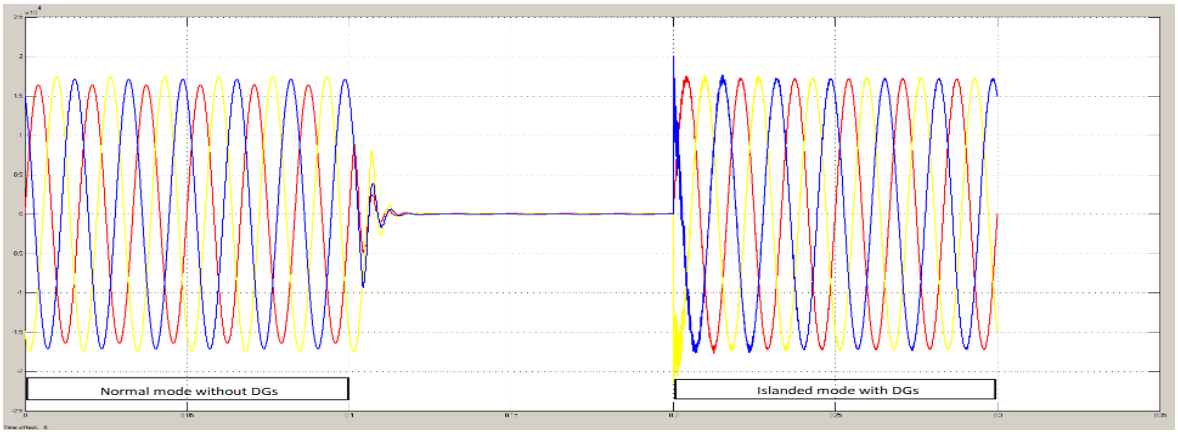

Figure 5.9: Voltage waveform of node-842 without and with the DGs

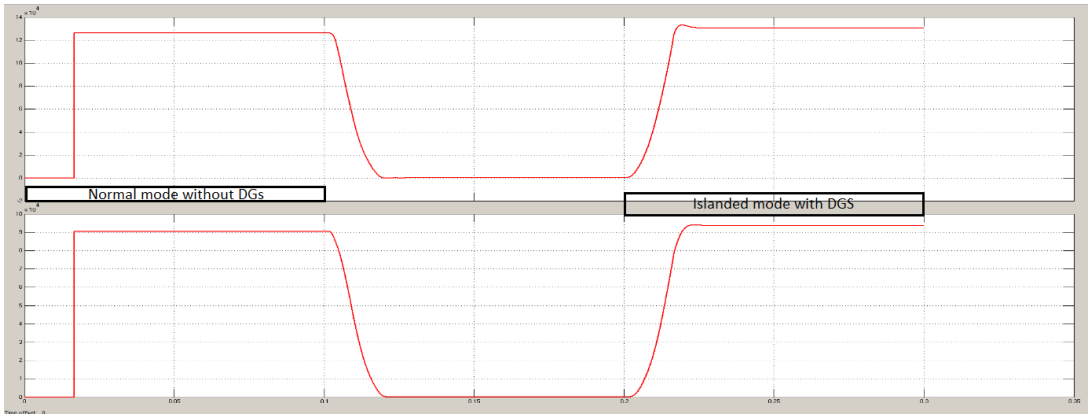

Figure 5.10: Active and Reactive power levels of node-842 without and with the DGs

Node-840

This is the node to which the first PV unit is connected. The voltage in this node before the DGs were switched on say phase-A was 0.8072 pu. In the islanding mode, when the DGs were on the voltage profile was 0.8508 pu in all the phases as shown in Figure 5.11. So, not only the voltage profile is improved by 5.4% and the voltage profile 0.8508 pu was available in every phase; a suitable situation since the node-840 is in the original sag end where the region was heavily loaded. Also, power flow through the node before the DGs were 104.69 kW and 52.324 kVAr respectively. With the DGs in the islanded mode, power flow through the

node was 107.82 kW and 48.034 kVAr respectively as shown in Figure 5.12.

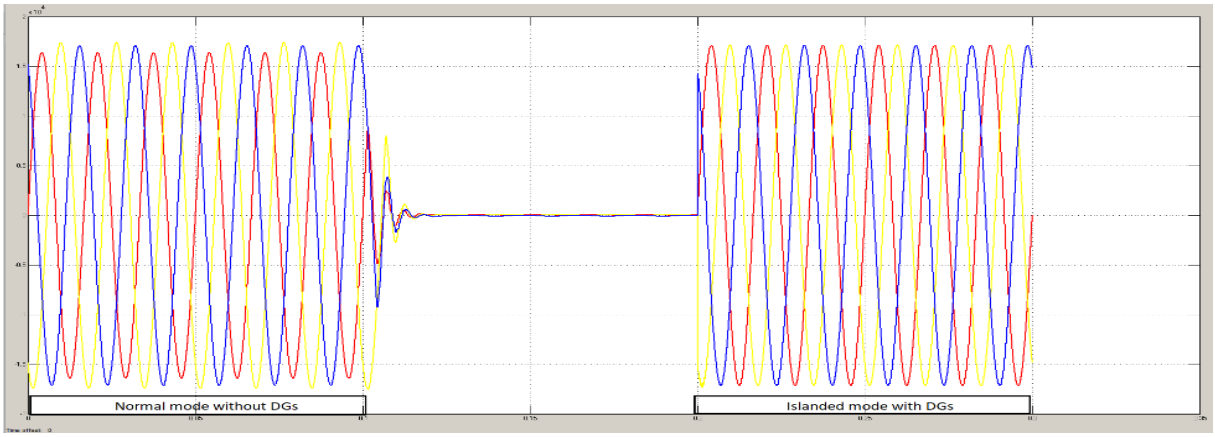

Figure 5.11: Voltage waveform of node-840 without and with the DGs

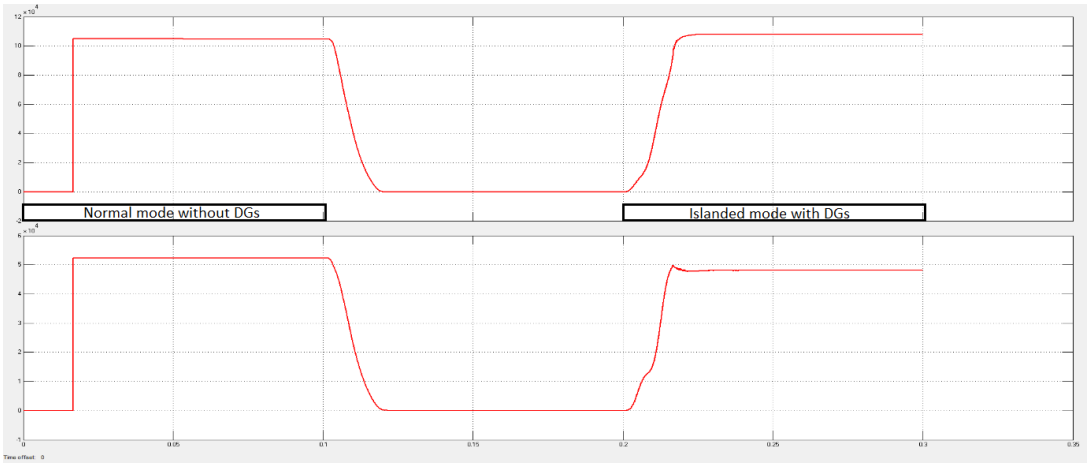

Figure 5.12: Active and Reactive power levels of node-840 without and with the DGs

5.3 CONCLUSION

Thus, in this chapter we see that with the use of PV units as DG sources the voltage profile is highly improved for the loads of the IEEE 34-node radial distribution feeder. The solution to delivering power to the loads is well found as the voltage profile is improved in this situation with about a 5% margin. Also, the loads in the sag end are having better voltage profile with the use of DGs and the choice of the locations where they were connected. The conclusion to this work is described in the next chapter.

CHAPTER 6

CONCLUSION AND FUTURE WORK

6.1 CONCLUSION

The real-time model of the IEEE 34-node distribution system was developed and simulated in the Simulink™ and OPAL-RT™ environments. Design of the system was itself a challenging one as the 34-node distribution system is a vast system where each nodes and elements were developed from scratch. The focus was made on the exact simulation of the system as tuned to the real world. Objectives were to study the behaviour of the system both in the desired state and the abnormal states. Study regarding islanding of the system was made in detail to study the feasibility of the design of the photovoltaic system which would cater the system during islanding mode and also to increase the overall voltage profile. It was observed that in islanded mode the photovoltaic system served well and maintained the power supply to the loads within commendable limitations of time. A drawback of this model, that was observed while running in OPAL-RT™ simulator, was that there were many numbers of overruns. Hence, this model needs further improvements so that overruns are avoided. This will help to integrate real-time hardwares along with this model.

6.2 FUTURE WORK

Though a lot of important milestones were achieved in this endeavour, a lot remains to be done to make the whole system more robust. More accurate designs will have to be introduced in the future to study the working of the OLTCs itself. Efforts are needed to be made so that there are zero overruns of the system in the OPAL-RT™ simulator. DG system not only contain PV systems but can contain hydro generators, wind farms and battery units. Storage is very important in the upcoming time which will be needed for seamless power source transition between several units

for designing modern amenities like smart-grid and smart-cities. Also, protection system are needed to be installed in order to quench the over-arching current surges which can cause harm to the system.

REFERENCES

1. IEEE Power & Energy Society (PES). Distribution test feeders. [Online] {Available} http://ewh.ieee.org/soc/pes/dsacom/testfeeders/ (Accessed: Dec 3, 2018).

2. N. Mwakabuta, and A. Shekar, "Comparative study of the IEEE 34 node test feeder under practical simplifications," in *Proc. 2-007 39th North American Power Symposium (NAPS 2007),* 2007, pp. 484-491.

3. J. O. Owuor, J. L. Munda, and A. A. Jimoh, "The IEEE 34 node test feeder as a simulation testbench for distributed generation," in *IEEE Africon 2011 – The Falls Resort and Conference Centre, Livingstone, Zamibia,* 13 – 15 September 2011.

4. S. P. Ashok, "Modelling and protection scheme for IEEE 34 radial distribution feeder with and without distributed generation," thesis for University of Wisconsin-Milwaukee, Paper 394, May 2014.

5. P. Singh, "Real-time modelling and simulation of distribution feeder and distributed resources," thesis for Colorado State University, Fort Collins, Colorado, Fall 2015.

6. Dr. A. Subburaj, A. R. Arra, and Dr. S. Bayne, "Stability Analysis of A.C. and D.C. microgrids using OPAL-Real Time Digital Simulator," in *Proc. Ninth Annual IEEE Green Technologies Conference,* 2017, pp. 39-45.

7. H. Hooshyar, F. Mahmood, L. Vanfretti, and M. Baudette, "Specification, implementation, and hardware-in-the-loop real-time simulation of an active distribution grid" in *Sustainable Energy and Networks*, Elsevier, September 2015, pp. 36-51.

8. D. P. Kothari and I. J. Nagrath, "Modern Power System Analysis", Tata McGraw-Hill Education, Third Edition, 2003.

9. Sonali Surawdhaniwar and Ritesh Diwan, "Study of Maximum Power Point Tracking Using Perturb and Observe Method" in *Proc. International Journal of Advanced Research in Computer Engineering & Technology,* Volume 1, Issue 5, July 2012, pp. 106-110.

10. Yinghua Dong, Jie Ding, Jingsheng Huang, Lianghui Xu and Wei Dong, "Investigation of PV Inverter MPPT Efficiency Test Platform", in *Proc. International Conference on Renewable Power Generation (RPG 2015),* 2015, Beijing, China.

11. Lloyd Dixon, “Average Current Mode Control of Switching Power Supplies”, Unitrode, U-140.

12. “Modelling and Control of dc/dc Boost Converter in FC systems”, ME 590 report to Professor Stefanopoulou from Wei Xi.

13. Jenica Ileana CORCAU and Pompiliu Constantinache, “Modeling and Control of High Power Inverters”, in Annals of the University of Craiova, Electrical Engineering series, No. 32, 2008; ISSN 1842-4805, pp. 257-260.

14. Mustapha Raoufi and Moulay Tahar Lamchich, “Average Current Mode Control of a Voltage Source Inverter connected to the Grid: Application to different Filter Cells”, in *Proc. Journal of Electrical Engineering, Vol. 55, No. 3-4,* 2004, pp. 77-82 [ISSN 1335-3632 ©2004 FEI STU].

15. Liang Che, Mohammad Shahidehpour, Ahmed Alabduwahab and Yusuf Al-Turki, “Hierarchical Coordination of a Community Microgrid With AC and DC Microgrids” in *Proc. IEEE Transactions on Smart Grid*, Volume 6, Issue 6, Nov. 2015.

16. Jatin Jangra and Shelly Vadhera, “Load Flow Analysis for Three Phase Unbalanced Distribution Feeders Using MATLAB”, in *Proc. 2017 2nd International Conference for Convergence in Technology (I2CT)*, 2017, pp. 862-866

17. Aasha Kapur Mehta (project director), Gadadhara Mohapatra, Akhtar Ali and Suparna Das Mukherjee, “Renewable Energy for Rural Livelihoods in MNRE-UNDP-FRG Project Villages in Rajasthan and Uttarakhand: A Report” by Indian Institute of Public Administration, New Delhi, 2009 sponsored by Ministry of New and Renewable Energy – Government of India.

Appendix A

A.1 IEEE 34 NODE TEST FEEDER DATA

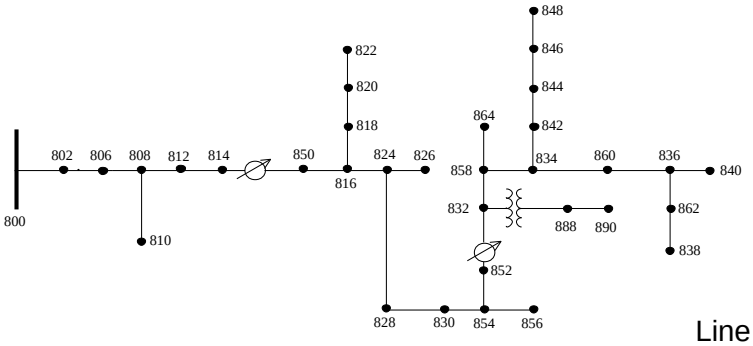

Overhead Line Configurations (Config.)

Config.	Phasing	Phase ACSR	Neutral ACSR	Spacing ID
300	B A C N	1/0	1/0	500
301	B A C N	#2 6/1	#2 6/1	500
302	A N	#4 6/1	#4 6/1	510
303	B N	#4 6/1	#4 6/1	510
304	B N	#2 6/1	#2 6/1	510

Line Segment Data

Node A	Node B	Length(ft.)	Config.
800	802	2580	300
802	806	1730	300
806	808	32230	300
808	810	5804	303
808	812	37500	300
812	814	29730	300
814	850	10	301
816	818	1710	302
816	824	10210	301
818	820	48150	302
820	822	13740	302
824	826	3030	303
824	828	840	301
828	830	20440	301
830	854	520	301
832	858	4900	301
832	888	0	XFM-1
834	860	2020	301
834	842	280	301
836	840	860	301
836	862	280	301
842	844	1350	301
844	846	3640	301
846	848	530	301
850	816	310	301
852	832	10	301
854	856	23330	303
854	852	36830	301
858	864	1620	302
858	834	5830	301
860	836	2680	301
862	838	4860	304
888	890	10560	300

Transformer Data

	kVA	kV-high	kV-low	R - %	X - %
Substation:	2500	69 - D	24.9 -Gr. W	1	8
XFM -1	500	24.9 - Gr.W	4.16 - Gr. W	1.9	4.08

Spot Loads

Node	Load Model	Ph-1 kW	Ph-1 kVAr	Ph-2 kW	Ph-2 kVAr	Ph-3 kW	Ph-4 kVAr
860	Y-PQ	20	16	20	16	20	16
840	Y-I	9	7	9	7	9	7
844	Y-Z	135	105	135	105	135	105
848	D-PQ	20	16	20	16	20	16
890	D-I	150	75	150	75	150	75
830	D-Z	10	5	10	5	25	10
Total		344	224	344	224	359	229

Distributed Loads

Node A	Node B	Load Model	Ph-1 kW	Ph-1 kVAr	Ph-2 kW	Ph-2 kVAr	Ph-3 kW	Ph-3 kVAr
802	806	Y-PQ	0	0	30	15	25	14
808	810	Y-I	0	0	16	8	0	0
818	820	Y-Z	34	17	0	0	0	0
820	822	Y-PQ	135	70	0	0	0	0
816	824	D-I	0	0	5	2	0	0
824	826	Y-I	0	0	40	20	0	0
824	828	Y-PQ	0	0	0	0	4	2
828	830	Y-PQ	7	3	0	0	0	0
854	856	Y-PQ	0	0	4	2	0	0
832	858	D-Z	7	3	2	1	6	3
858	864	Y-PQ	2	1	0	0	0	0
858	834	D-PQ	4	2	15	8	13	7
834	860	D-Z	16	8	20	10	110	55
860	836	D-PQ	30	15	10	6	42	22
836	840	D-I	18	9	22	11	0	0
862	838	Y-PQ	0	0	28	14	0	0
842	844	Y-PQ	9	5	0	0	0	0
844	846	Y-PQ	0	0	25	12	20	11
846	848	Y-PQ	0	0	23	11	0	0
Total			262	133	240	120	220	114

Shunt Capacitors

Node	Ph-A kVAr	Ph-B kVAr	Ph-C kVAr
844	100	100	100
848	150	150	150
Total	250	250	250

Regulator Data

Regulator ID:	1		
Line Segment:	814 - 850		
Location:	814		
Phases:	A - B -C		
Connection:	3-Ph,LG		
Monitoring Phase:	A-B-C		
Bandwidth:	2.0 volts		
PT Ratio:	120		
Primary CT Rating:	100		
Compensator Settings:	Ph-A	Ph-B	Ph-C
R - Setting:	2.7	2.7	2.7
X - Setting:	1.6	1.6	1.6
Volltage Level:	122	122	122

Regulator ID:	2		
Line Segment:	852 - 832		
Location:	852		
Phases:	A - B -C		
Connection:	3-Ph,LG		
Monitoring Phase:	A-B-C		
Bandwidth:	2.0 volts		
PT Ratio:	120		
Primary CT Rating:	100		
Compensator Settings:	Ph-A	Ph-B	Ph-C
R - Setting:	2.5	2.5	2.5
X - Setting:	1.5	1.5	1.5
Volltage Level:	124	124	124

Line Impedances

```
--------- Z & B Matrices Before Changes ---------
Configuration 300:

          Z (R +jX) in ohms per mile
 1.3368  1.3343   0.2101  0.5779   0.2130  0.5015
                  1.3238  1.3569   0.2066  0.4591
                                   1.3294  1.3471
          B in micro Siemens per mile
            5.3350   -1.5313   -0.9943
                      5.0979   -0.6212
                                4.8880
Configuration 301:

          Z (R +jX) in ohms per mile
 1.9300  1.4115   0.2327  0.6442   0.2359  0.5691
                  1.9157  1.4281   0.2288  0.5238
                                   1.9219  1.4209
          B in micro Siemens per mile
            5.1207   -1.4364   -0.9402
                      4.9055   -0.5951
                                4.7154

Configuration 302:

          Z (R +jX) in ohms per mile
 2.7995  1.4855   0.0000  0.0000   0.0000  0.0000
                  0.0000  0.0000   0.0000  0.0000
                                   0.0000  0.0000
          B in micro Siemens per mile
            4.2251    0.0000    0.0000
                      0.0000    0.0000
                                0.0000
```

Configuration 303:

Z (R +jX) in ohms per mile

0.0000	0.0000	0.0000	0.0000	0.0000	0.0000
		2.7995	1.4855	0.0000	0.0000
				0.0000	0.0000

B in micro Siemens per mile

0.0000	0.0000	0.0000
	4.2251	0.0000
		0.0000

Configuration 304:

Z (R +jX) in ohms per mile

0.0000	0.0000	0.0000	0.0000	0.0000	0.0000
		1.9217	1.4212	0.0000	0.0000
				0.0000	0.0000

B in micro Siemens per mile

0.0000	0.0000	0.0000
	4.3637	0.0000
		0.0000

A.2 SIMULINK™ AND RT-LAB™ VERSIONS

```
--------------------------------------------------------------------------------
MATLAB Version: 8.1.0.604 (R2013a)
MATLAB License Number: 874166
Operating System: Microsoft Windows 10 Home Version 1809 (Build 17763.437)
Java Version: Java 1.6.0_17-b04 with Sun Microsystems Inc.
Java HotSpot(TM) Client VM mixed mode

--------------------------------------------------------------------------------
```

MATLAB	Version 8.1	(R2013a)
Simulink	Version 8.1	(R2013a)
Aerospace Blockset	Version 3.11	(R2013a)
Aerospace Toolbox	Version 2.11	(R2013a)
Bioinformatics Toolbox	Version 4.3	(R2013a)
Communications System Toolbox	Version 5.4	(R2013a)
Computer Vision System Toolbox	Version 5.2	(R2013a)
Control System Toolbox	Version 9.5	(R2013a)
Curve Fitting Toolbox	Version 3.3.1	(R2013a)
DO Qualification Kit	Version 2.1	(R2013a)
DSP System Toolbox	Version 8.4	(R2013a)
Data Acquisition Toolbox	Version 3.3	(R2013a)
Database Toolbox	Version 4.1	(R2013a)
Datafeed Toolbox	Version 4.5	(R2013a)
Econometrics Toolbox	Version 2.3	(R2013a)
Embedded Coder	Version 6.4	(R2013a)
Filter Design HDL Coder	Version 2.9.3	(R2013a)
Financial Instruments Toolbox	Version 1.1	(R2013a)
Financial Toolbox	Version 5.1	(R2013a)
Fixed-Point Designer	Version 4.0	(R2013a)
Fuzzy Logic Toolbox	Version 2.2.17	(R2013a)
Gauges Blockset	Version 2.0.7	(R2013a)
Global Optimization Toolbox	Version 3.2.3	(R2013a)
HDL Coder	Version 3.2	(R2013a)
HDL Verifier	Version 4.2	(R2013a)
IEC Certification Kit	Version 3.1	(R2013a)
Image Acquisition Toolbox	Version 4.5	(R2013a)
Image Processing Toolbox	Version 8.2	(R2013a)
Instrument Control Toolbox	Version 3.3	(R2013a)
MATLAB Builder EX	Version 2.3.1	(R2013a)
MATLAB Builder JA	Version 2.2.6	(R2013a)
MATLAB Builder NE	Version 4.1.3	(R2013a)
MATLAB Coder	Version 2.4	(R2013a)
MATLAB Compiler	Version 4.18.1	(R2013a)
MATLAB Report Generator	Version 3.14	(R2013a)

Mapping Toolbox	Version 3.7	(R2013a)
Model Predictive Control Toolbox	Version 4.1.2	(R2013a)
Model-Based Calibration Toolbox	Version 4.6	(R2013a)
Neural Network Toolbox	Version 8.0.1	(R2013a)
OPC Toolbox	Version 3.2	(R2013a)
Optimization Toolbox	Version 6.3	(R2013a)
Parallel Computing Toolbox	Version 6.2	(R2013a)
Partial Differential Equation Toolbox	Version 1.2	(R2013a)
Phased Array System Toolbox	Version 2.0	(R2013a)
RF Toolbox	Version 2.12	(R2013a)
RT-LAB	Version v11.0.5.499	
(R2013a.x)		
Real-Time Windows Target	Version 4.2	(R2013a)
Robust Control Toolbox	Version 4.3	(R2013a)
Signal Processing Toolbox	Version 6.19	(R2013a)
SimBiology	Version 4.3	(R2013a)
SimDriveline	Version 2.4	(R2013a)
SimElectronics	Version 2.3	(R2013a)
SimEvents	Version 4.3	(R2013a)
SimHydraulics	Version 1.12	(R2013a)
SimMechanics	Version 4.2	(R2013a)
SimPowerSystems	Version 5.8	(R2013a)
SimRF	Version 4.0	(R2013a)
Simscape	Version 3.9	(R2013a)
Simulink 3D Animation	Version 6.3	(R2013a)
Simulink Code Inspector	Version 1.3	(R2013a)
Simulink Coder	Version 8.4	(R2013a)
Simulink Control Design	Version 3.7	(R2013a)
Simulink Design Optimization	Version 2.3	(R2013a)
Simulink Design Verifier	Version 2.4	(R2013a)
Simulink PLC Coder	Version 1.5	(R2013a)
Simulink Report Generator	Version 3.14	(R2013a)
Simulink Verification and Validation	Version 3.5	(R2013a)
Spreadsheet Link EX	Version 3.1.7	(R2013a)
Stateflow	Version 8.1	(R2013a)
Statistics Toolbox	Version 8.2	(R2013a)
Symbolic Math Toolbox	Version 5.10	(R2013a)
System Identification Toolbox	Version 8.2	(R2013a)
SystemTest	Version 2.6.5	(R2013a)
Trading Toolbox	Version 1.0	(R2013a)
Vehicle Network Toolbox	Version 2.0	(R2013a)
Wavelet Toolbox	Version 4.11	(R2013a)
xPC Target	Version 5.4	(R2013a)
xPC Target Embedded Option	Version 5.4	(R2013a)

A.3 DISTRIBUTED PARAMETER CALCULATIONS

The data for the line segments is given in the form of impedance matrix and admittance matrix with specific configurations. In order to incorporate it in our model, we need to separate it in impedance matrix and mutual- and self-capacitances. Such an example is taken for line configuration 300 and the configuration process is shown below.

Configuration 300:

```
          Z (R +jX) in ohms per mile
 1.3368   1.3343    0.2101   0.5779    0.2130   0.5015
                    1.3238   1.3569    0.2066   0.4591
                                       1.3294   1.3471

          B in micro Siemens per mile
            5.3350   -1.5313   -0.9943
                      5.0979   -0.6212
                                4.8880
```

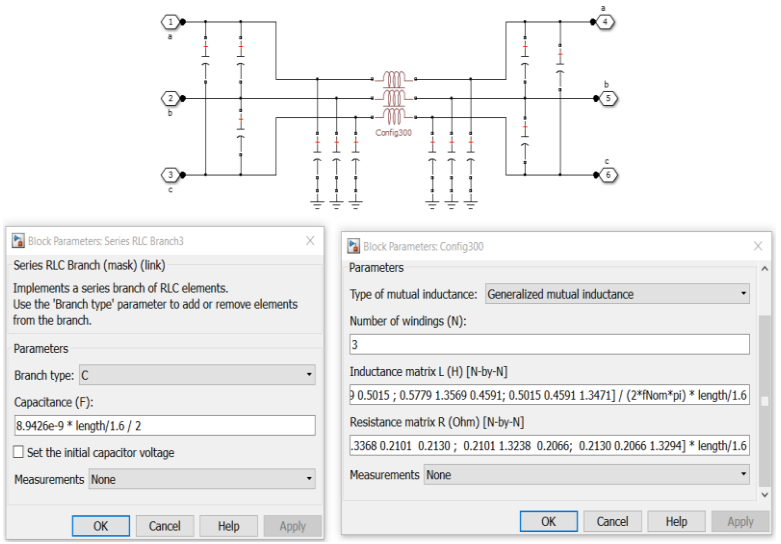

For the inductance and resistance associated with it, the matrices were set in the parameters as it without any modification by separating [R + jX] matrix as [R] and [X] matrices respectively.

While this was set the values of the mutual- and self-capacitances were calculated individually as follows:

$B_{A0} = b_{AA} + b_{AB} + b_{AC}$

$= 5.3350 - 1.5313 - 0.9943$ µSiemens

$= 2.8094$ µSiemens

$C_A = B_{A0} / (2 * \pi * f_{system})$

$= 2.8094 * 10^{-6} / (2 * \pi * 50)$

$= 8.9426$ nC

$B_{B0} = b_{BB} + b_{AB} + b_{BC}$

$= 5.0979 - 1.5313 - 0.6212$ µSiemens

$= 2.9454$ µSiemens

$C_B = B_{B0} / (2 * \pi * f_{system})$

$= 2.9454 * 10^{-6} / (2 * \pi * 50)$

$= 9.3755$ nC

$B_{C0} = b_{CC} + b_{AC} + b_{BC}$

$= 4.8880 - 0.9943 - 0.6212$ µSiemens

$= 3.2725$ µSiemens

$C_C = B_{C0} / (2 * \pi * f_{system})$

$= 3.2725 * 10^{-6} / (2 * \pi * 50)$

$= 0.0104$ nC

$B_{AB} = 1.5313$ µSiemens

$C_{AB} = 1.5313 * 10^{-6} / (2 * \pi * 50)$

$= 4.8743$ nC

$B_{BC} = 0.6212$ µSiemens

$C_{BC} = 0.6212 * 10^{-6} / (2 * \pi * 50)$

$= 1.9773$ nC

$B_{AC} = 0.9943$ µSiemens

$C_{BC} = 0.9943 * 10^{-6} / (2 * \pi * 50)$

$= 3.1650$ nC

And so on for other types of configurations too.

A.4 MAXIMUM POWER POINT TRACKING ALGORITHM

The following algorithm is used for implementing the 'perturb and observe' method in the Simulink™ block for MPPT.

```
% Simple MPP "perturb and observe" tracking algorithm
% using Boost DC-DC input current Iref as the control variable
% Pold, Iref and Increment are initialized in InitializeMPPtrackIref.m
% Input: power P to be maximized
% Output: reference current
function y = MPPtrackIref(P, Irefmp)

persistent Pold;
if isempty(Pold)
Pold = 0;
end

persistent Iref;
if isempty(Iref)
Iref = Irefmp;
end

persistent Increment;
if isempty(Increment)
Increment = 1;
end

% global Pold;
% global Iref;
% global Increment;

IrefH = 5; % upper limit for the reference current
IrefL = 0; % lower limit for the reference current
DeltaI = 0.01; % reference current increment

if (P < Pold)
    Increment = -Increment; % change direction if P decreased
end

if (P == 0)
    Increment = -Increment; % change direction if P decreased
end

if (P == Pold)
    Iref=Iref;
else

% increment current reference
Iref=Iref+Increment*DeltaI;
end

% check for upper limit
if (Iref > IrefH)
    Iref = IrefH;
end

% check for lower limit
if (Iref < IrefL)
    Iref = IrefL;
end

% save power value
Pold = P;
% output current reference
y = Iref;
```